Biologically agglutinated eukaryotic microfossil from Cryogenian cap carbonates

Citation: Moore, K. R., T. Bosak, F. A. Macdonald, D. J. G. Lahr, S. Newman, C. Settens, and S. B. Pruss. "Biologically Agglutinated Eukaryotic Microfossil from Cryogenian Cap Carbonates." Geobiology 15, no. 4 (January 6, 2017): 499–515.

As Published: https://doi.org/10.1111/gbi.12225

Persistent URL: http://hdl.handle.net/1721.1/119676

Version: Author's final manuscript: final author's manuscript post peer review, without publisher's formatting or copy editing

BIOLOGICALLY AGGLUTINATED EUKARYOTIC MICROFOSSIL FROM CRYOGENIAN CAP CARBONATES

KELSEY R. MOORE[1], TANJA BOSAK[1], FRANCIS A. MACDONALD[2], DANIEL J. G. LAHR[3], SHARON NEWMAN[1], CHARLES SETTENS[4], SARA B. PRUSS[5*]

[1] *The Department of Earth, Atmospheric and Planetary Sciences, Massachusetts Institute of Technology, Cambridge, MA 02139, USA, krmoore@mit.edu;* [2] *The Department of Earth and Planetary Sciences, Harvard University, Cambridge, MA 02138, USA, fmacdon@fas.harvard.edu;* [3] *Department of Zoology, University of São Paulo, São Paulo SP 05508-90, Brazil, dlahr@ib.usp.br,* [4] *Center for Materials Science and Engineering, Massachusetts Institute of Technology, Cambridge, MA 02139, USA, settens@mit.edu;* [5] *Department of Geosciences, Smith College, Northampton, MA 01063, USA, spruss@smith.edu*

*Corresponding author

Keywords: microfossil, agglutinated, tests, Cryogenian, Sturtian, Kakontwe, Taishir

ABSTRACT

Cryogenian cap carbonates that overlie Sturtian glacial deposits were formed during a post-glacial transgression. Here we describe microfossils from the Kakontwe Formation of Zambia and the Taishir Formation of Mongolia—both Cryogenian age, post-Sturtian cap carbonates—and investigate processes involved in their formation and

preservation. We compare microfossils from these two localities to an assemblage of well-documented microfossils previously described in the post-Sturtian Rasthof Formation of Namibia. Microfossils from both new localities have 10 +/- 1 µm thick walls composed of carbonaceous matter and aluminosilicate minerals. Those found in the Kakontwe Formation are spherical or ovoid and 90 +/- 5 µm to 200 +/- 5 µm wide. Structures found in the Taishir Formation are mostly spherical, 50 +/- 5 µm to 140 +/- 5 µm wide, with distinct features such as blunt or concave edges. Chemical and mineralogical analyses show that the walled structures and the clay fraction extracted from the surrounding sediments are composed of clay minerals, especially muscovite and illite, as well as quartz, iron and titanium oxides, and some dolomite and feldspar. At each locality, the mineralogy of the microfossil walls matched that of the clay fractions or the surrounding sediment. The abundance of these minerals in the walled microfossils relative to the surrounding carbonate matrix and microbial laminae, and the presence of minerals that cannot precipitate from solution (titanium oxide and feldspar), suggests that the composition represents the original mineralogy of the structures. Furthermore, the consistency in mineralogy of both microfossils and sediments across the three basins, and the uniformity of size and shape among mineral grains in the fossil walls indicate that these organisms incorporated these minerals by primary biological agglutination. The discovery of new, mineral-rich microfossil assemblages in microbially laminated and other fine-grained facies of Cryogenian cap carbonates from multiple localities on different paleo-continents demonstrates that agglutinating eukaryotes were widespread in carbonate-dominated marine environments in the aftermath of the Sturtian glaciation.

INTRODUCTION

During the Cryogenian, the Earth experienced unparalleled climatic extremes in which global glaciations were followed by intervals of extreme warming (e.g., Hoffman *et al.*, 1998; Pierrehumbert *et al.*, 2011). Geological evidence suggests that ice existed at sea level near the equator during two intervals of the Neoproterozoic: the Sturtian (~717-660 Ma), and the Marinoan (>640-635 Ma) (Rooney *et al.*, 2015). Cap carbonates—globally occurring carbonates with unusual sedimentological features (e.g., Hoffman and Schrag, 2002; Hoffman et al., 2011; Pruss et al., 2010)—sit atop both glacial deposits, and record the post-glacial warming interval.

Prior to the Sturtian glaciation, several groups of eukaryotes are known to have radiated, including amoebae and both red and green algae (Knoll, 1992; Butterfield and Rainbird, 1998; Butterfield, 2000; Cohen and Macdonald, 2015). Molecular clocks also indicate the radiation of other modern eukaryotic groups such as foraminifera, ciliates and animals prior to the Snowball Earth event (Parfrey *et al.*, 2011). The Sturtian glaciation is speculated to have caused large scale extinctions especially of eukaryotic communities (Corsetti *et al.*, 2003), resulting in dramatic change in marine ecology after the Sturtian glaciation. Indeed, the harsh conditions during this global glaciation and its long duration may have stressed the mostly microbial ecosystems at this time (Cohen and Macdonald, 2015). For example, the presence of glaciers extending to the equator 700-1400 m thick on the continents (Liu and Peltier, 2010) and ~1000 m thick on the oceans (Tziperman et al., 2012) may have caused a shortage of liquid water and reduced the availability of sunlight in the ocean, especially impacting photosynthetic organisms including new communities of eukaryotes (Costas *et al.*, 2008). The extent of these impacts, however, has been poorly understood. Previous work on Sturtian glacial diamictites and shales deposited during the Cryogenian nonglacial interlude in Australia and Svalbard has suggested that

eukaryotic diversity decreased in the aftermath of the Sturtian glaciation (Riedman et al., 2014). Cohen and Macdonald (2015) also point out that the fossil record during the Cryogenian shows an apparent decrease in eukaryotic diversity, but they suggest that this decrease in diversity is not statistically significant and may be an artifact.

The fossil record of carbonate sediments deposited in the aftermath of the Sturtian glaciation may offer new insights into marine ecology during the Cryogenian non-glacial interlude and processes involved in the formation and preservation of these fossils. The geochemistry, sedimentology, and stratigraphy of cap carbonates are well studied (Macdonald et al., 2009; Wendorff and Key, 2009; Master and Wendorff, 2011; Johnston et al., 2012; Bold et al., 2016), but only recently has a fossil record emerged from these units. Investigation of the Rasthof Formation of Namibia—a post-Sturtian cap carbonate—revealed abundant agglutinated testate microfossils (Bosak *et al.*, 2011; Bosak *et al.*, 2012; Dalton *et al.*, 2013). The microfossil assemblages of the Rasthof Formation contain agglutinated oval and spherical tests whose morphologies are consistent with those of modern agglutinated testate amoebae (Bosak *et al.*, 2011). Also present in these cap carbonates are agglutinated, tubular forms and some oval structures longer than 200 μm with blunt ends which resemble modern monothalamous tubular and globular foraminiferans (Bosak *et al.*, 2011; Bosak *et al.*, 2012). Additional elongated structures, 50 μm to 175 μm long, resembling modern codonellid tintinnid ciliates, are present in the Taishir Formation of Mongolia (Bosak *et al.*, 2011). These were the first reported microfossils in cap carbonates, but the question remains how these structures were formed and preserved, and whether these fossils are representative of a global biological picture during the non-glacial interval.

Here, we describe new microfossil assemblages from post-Sturtian cap carbonates of the Kakontwe Formation of Zambia and the Taishir Formation of Mongolia, and compare these fossils to testate microfossils from the Rasthof Formation of Namibia. The new fossil assemblages consist primarily of simple morphotypes, but some also contain distinct and previously unrecorded features, increasing the total morphological diversity and bolstering global distribution of these eukaryotic organisms in the aftermath of the Sturtian glaciation. We also present compositional and mineralogical analyses of the mineral-rich, walled microfossils from different localities across the three formations to test hypotheses about the roles of biological agglutination and diagenetic processes in fossil preservation.

GEOLOGICAL SETTING

The Kakontwe Formation, Zambia

The Neoproterozoic Katangan Supergroup spans the Katangan Province of Democratic Republic of Congo, Zambia, and eastern Angola and was deposited in an intercratonic rift (Master and Wendorff, 2011). The Katangan Supergroup includes (from bottom to top) the Roan, Nguba, Kundelungu, Fungurume, and Plateau groups (Batumike et al., 2007; Master and Wendorff, 2011; Rooney et al., 2015). At the base of the Nguba Group lies the Grand Conglomerat, a glacial diamictite of Sturtian age (Batumike et al., 2007; Master and Wendorff, 2011; Rooney et al., 2015). The Grand Conglomerat is overlain conformably by the Kakontwe Formation, a post-glacial cap carbonate (Wendorff and Key, 2009; Master and Wendorff, 2011; Rooney et al., 2015). Near the town of Kakontwe, this unit is approximately 245 m thick. Massive grey dolomite at the base is overlain by massive grey limestone with local oncolites, bedded grey limestone, light grey to black massive dolomitic limestone and dark grey limestone

interbedded with dark shaley limestone (Batumike et al., 2007; Rooney et al., 2015). Near the town of Kipushi, the Kakontwe Limestone is thicker (~340 m) and is a medium- to coarse-grained dolostone rather than the limestone found to the north (Batumike et al., 2007).

Samples of the Kakontwe Formation were collected from core drilled near Kipushi, Democratic Republic of Congo. Details of the location of the drill core and core log can be found in Bodiselitsch et al. (2005). We analyzed 19 samples spanning ~85 m of stratigraphy (from 54 m to 139 m) (Figure 1A). In this part of the section, the Kakontwe Formation is dominated by dark, micritic, thinly-laminated microbialaminite. The microbial lamination in these dark limestones exhibited varying degrees of preservation, and 15 samples out of 19 yielded microfossils.

The Taishir Formation, Mongolia

The Cryogenian Tsagaan Olom Group, which hosts the Taishir Formation, covers the Zavkhan Terrane of southwestern Mongolia and represents mostly carbonate ramp deposition (Macdonald et al., 2009; Bold et al., 2016). The Tsagaan Olom Group contains glacial deposits of the Maikhan-Uul diamictite, thought to correspond to the Sturtian glaciation (Shields and Veizer, 2002; Macdonald et al., 2009; Bosak et al., 2011b). This diamictite is overlain by the Taishir Formation.

The Taishir Formation is a post-Sturtian organic-rich limestone approximately 570 m thick (Macdonald et al., 2009; Johnston et al., 2012; Bold et al., 2016) and can be divided into three supersequences. The first supersequence (unit T1) is 110 m thick and consists of a dark grey laminated limestone followed by calcisilite and grainstone(Bold et al., 2016). The second super sequence (unit T2) is 210 m thick and begins with thin bedded micrite and calcisilite succeeded

by meter-scale parasequences of calcisilite and grainstone. The base of the third supersequence is defined by a recessive interval composed of thin-bedded micrite and calcisilite followed by a sequence of dark limestone micrite, calcisilite, grainstone with giant ooids, and minor microbialaminite. In total, the third supersequence (unit T3) is up to 250 m thick (Bold et al., 2016).

Samples of the Taishir Formation are from South Khukh Davaa (section F1125) and span the lower 42 m of unit T1 (Figure 1B). Details of the location and stratigraphy of this section are provided in Bold et al. (2016). Samples from this locality include light grey, thinly laminated limestone and massive dark micritic limestones. In total, we examined 18 samples from the massive limestone, 8 of which yielded microfossils.

METHODS

Nineteen samples from the Kakontwe Formation and 18 samples from the Taishir Formation were dissolved to search for microfossils. Fifteen previously analyzed fossiliferous samples of the Rashtof Formation were also dissolved to collect microfossils for comparative analysis. Approximately 2.0 to 10.0 g of each sample were treated with 10% HCl to remove surficial contamination and the samples were subsequently dissolved in 10% acetic acid buffered by 0.65 M hydrated ammonium acetate to gently remove the carbonate matrix (e.g., Dalton *et al.*, 2013). Residues were filtered by suction filtration through 0.2 µm, 41µm, and 100 µm Millipore nylon net filters (EMD Millipore, HNWP04700, NY4104700, and NY1H04700, Billerica, MA, USA). Residues in the >100 µm range and the 41-100 µm range were examined under a Nikon SMZ645 stereoscopic microscope. Microfossils and any structures with repeating morphologies were picked from residues for analysis using scanning electron microscopy (SEM), SEM energy

dispersive X-ray spectrometry (SEM-EDS), X-ray diffraction (XRD), and Raman spectroscopy (instrument specifications below). Of the 37 new samples analyzed in this study, 23 yielded microfossils. Depending on the number of structures found in the residue covering a glass slide with dimensions 1" by 2" (*sensu* Dalton *et al.,* 2013), the samples were categorized as having abundant (>10 specimens), present (1-10 specimens) or no microfossils. These classifications were based on number of microfossils found in ~300 μL of residue. Thin sections of fossiliferous samples from the Kakontwe and Taishir formations were imaged using a petrographic microscope.

Potential microfossils were placed on SEM stubs (Ted Pella, Inc.) using carbon adhesive tabs and coated with gold and palladium using a Hummer V Sputter Coater (Smith College and Harvard University Center for Nanoscale Systems). Images were taken on the FEI Quanta 450 Scanning Electron Microscope at Smith College and the Ultra 55 FESEM at the Harvard University Center for Nanoscale Systems using a 5kV acceleration voltage. Measurements of 100 microfossils from one sample of the Kakontwe Formation and 50 microfossils from one sample from the Taishir Formation provided representative size distributions of microfossils from these localities. EDS Team software on the Supra 55 VP FESEM was used in conjunction with the 15 kV and 20 kV acceleration voltage to analyze the elemental composition through both points and maps on microfossils. We analyzed 13 specimens from the Kakontwe Formation, 8 from the Taishir Formation, and 7 from the Rasthof Formation using point analyses. Chemical composition maps were generated for one representative specimen from each formation. To compare the composition of internal and external surfaces of structures, a broken specimen from the Kakontwe Formation was analyzed through point analysis of one point from the interior surface and one from the exterior surface the structure.

To compare the minerals coating the microfossils (> 41 μm fraction) to those in the clay fraction of the residue, we obtained clay minerals from the 0.2 μm fraction of filtered residues and collected microfossils from the larger fractions using a fine paint brush (~10 μL per sample from each basin). Separate samples of the 0.2 μm fraction of filtered residues and microfossils were suspended in 70% ethanol and analyzed using XRD. Samples were dropped onto zero background quartz plates and left overnight to dry. Zero background plates containing samples were placed on a rotating stage in the PANalytical X'Pert PRO XRPD in the Center for Materials Science and Engineering at MIT. X-ray diffraction spectra were collected for each sample from 3 to 80 degrees over 4 to 7 hours and analyzed using HighScore Plus software.

Raman spectroscopy was performed using a Horiba Multiline Raman Spectrometer at the Center for Nanoscale Systems (Harvard University). Microfossil specimens from the Taishir and Kakontwe formations were placed on glass slides. The spectra of individual specimens were collected using 50X magnification with a 633 nm wavelength laser and the data were analyzed with LabSpec software.

Analyses of residues and individual specimens were combined with the analyses of 19 thin sections of samples from Kakontwe and 8 from the Taishir Formation. Each thin section was examined to confirm the presence of microfossils *in situ* in the rock samples and to compare the abundances and morphologies of microfossils between thin sections and residues. Thin sections were also used to further understand and mineralogy and preservation of microfossils within the carbonate and microbial sediments.

RESULTS

Acid Maceration, SEM Analysis and Size Distribution

Kakontwe Formation

Of the 19 insoluble residues analyzed from the Kakontwe Formation, 15 yielded putative microfossils (Table 1). Grey to black structures with repeating morphologies similar to the previously described microfossils from the Rasthof Formation and the Taishir Formation (Pruss et al., 2010; Bosak et al., 2011a, 2012; Dalton et al., 2013) were especially abundant in lower microbially laminated and unlaminated limestones. Samples K1-54.10 through K9-91.53 had abundant putative microfossils (more than 10 specimens per slide, Table 1). The only exception was sample K8-84.85, which did not contain any structures in residues. In samples K11-102.46 through K19-136.91, structures were present but less abundant (between 1 and 10 structures per slide, see Figure 1A, Table 1).

The diameters of structures from all samples ranged from 90 +/- 5 μm to 200 +/- 5 μm (Figure 2). When examined using SEM, most structures were ovoid (~48%, N=164; e.g. Figure 2A and B) and spherical (~16%; e.g. Figure 2C and D). Some structures also tapered to a narrow edge (~8.3%; Figure 2B), exhibited distinct blunt edges along the shorter axis (~7.6%, Figure 2C), or had spherical forms with an inwardly curved edge (~6.9%; Figure 2D) and possible openings (~13.2%, Figure 2B and E). The round surface of structures with inwardly curved edges transitioned smoothly into a concave surface lacking any breaks or fractures, indicating that the concave portion was a primary feature of the biologically created structure. Mineral grains 5 +/- 1 μm to 30 +/- 1 μm wide were uniformly distributed on the surfaces of structures (Figure 2). Broken or fractured structures revealed hollow interiors and 10 +/- 1 μm thick walls (5 broken specimens were analyzed under SEM, Figure 2H).

The size distribution of a representative assemblage of putative microfossils was determined in sample K2-58.25 because this sample contained abundant structures with

repeating morphologies (Table 1). One hundred putative microfossils were measured along both the long axis (length) and short axis (width). The lengths were normally distributed with a mean and median of 135 +/- 5 μm and a range of 90 +/- 5 μm to 200 +/- 5 μm (Figure 3). The widths were distributed bimodally, with modes at 135 +/- 5 μm and 110 +/- 5 μm. The bimodal distribution of widths results from the presence of both spherical and ovoid structures.

Taishir Formation

Fossiliferous samples from the Taishir Formation span ~4.5 meters near the base of the formation. Eight out of 16 samples of unlaminated dark micritic limestones between 6 m and 10.5 m from the base of the formation contained putative microfossils (Figure 1B, Table 1). Samples F1125-6.0 through F1125-10.5 consistently contained abundant structures (>10 putative microfossils per slide; See Table 1).

Residues of the Taishir Formation contained distinctly round structures that were smaller than those observed in the Kakontwe Formation (50 +/- 5 μm to 140 +/- 5 μm). Distinct, repetitive morphologies included predominantly spherical forms (~64%, N=95; Figure 4A), spherical forms with one blunt or inwardly curved end (~16%; Figure 4B, C, D, and E), forms that tapered along the long axis to a narrow end (~3.9%), ovoid forms (~6.5%), and spherical structures with a possible opening (~10%, Figure 4A, F, G, and H). All examined broken structures were hollow and had 8 +/- 1 μm thick walls (Figure 4H). The walls of structures from the Taishir Formation contained evenly distributed, 4 +/- 1 μm to 20 +/- 5 μm wide mineral grains.

We analyzed the size distribution of 50 structures from sample F1125-7.0 as a representative assemblage with abundant structures (Table 1). Both the lengths and the widths of

these specimens were skewed right, with a mean of 75 +/- 5 μm, a median of 90 +/- 5 μm and a range of 50 +/- 5 μm to 140 +/- 5 μm (Figure 3). The skew of the size distribution indicated a greater frequency of smaller structures (Figure 3).

Rasthof Formation

All 8 samples of dark micritic limestones from the Rasthof Formation from the Okaaru locality and 5 of the 7 samples from the Ongongo locality yielded structures similar to the previously described microfossils from different samples from these localities (Table 1, Dalton *et al.,* 2013; Bosak, *et al.,* 2011). These structures appeared predominantly in microbially laminated limestone samples, especially those with roll-up structures.

Putative microfossils from both Okaaru and Ongongo samples were white with red spots under reflected light (see Dalton et al., 2013). Structures were commonly ovoid (~27%, N=30; Figure 5A) and often had a blunt or curved edge (~27%). Additional forms were spherical (~14%; Figure 5B), tapered along the long axis to a narrow end (~14%), or had a hood and possible opening (~18%, Figure 5B, C, D, and E). All structures were uniformly coated by 4 +/- 1 μm to 20 +/- 1μm wide mineral grains (Figure 5). Rare broken structures revealed hollow interiors with 10 +/- 5 μm thick walls (Figure 5F).

Petrographic Analysis

Kakontwe Formation

Walled, mineral-coated structures could be seen in the thin sections of all 15 samples that yielded putative microfossils in residue. In thin section, structures appeared oval or circular, and had sizes consistent with those seen in residues (90 +/- 5 μm to 200 +/- 5 μm, Figure 6A, B). In

both microbially laminated and unlaminated limestone facies, structures often occurred in clusters throughout thin sections and were typically surrounded by matrix rather than cement (Figure 6A, B). The forms commonly appeared to be uniformly dark and micritic, but some had a dark outer wall (10 +/- 1 μm) and a micritic infill (Figure 6B). Occasionally, forms tapered along the long axis toward a blunt end or neck (not shown).

In general, samples with abundant or present microfossils in residues contained visible microfossils in their corresponding thin sections. However, thin sections of 2 samples, K14-115.00 and K19-136.91, revealed more structures than their corresponding residues: ~20 structures were present in thin sections, while residues contained <10 structures per slide. Both K14-115.00 and K19-136.91 facies had disrupted fabrics and appeared to be recrystallized. In these facies, structures seen in thin section appeared to be altered and contained more carbonate cement inside of the structure than structures in other samples. This suggests that microfossils from these samples may have been destroyed in the acid maceration process, explaining their absence in residues.

Taishir Formation

Thin sections of the Taishir Formation contained spherical forms whose sizes and round, blunt-edged and elongated morphologies were consistent with the structures found in residue (50 +/- 5 μm to 140 +/- 5 μm). Grey structures were most visible in dark, fine-grained limestone facies and were often filled with micrite (Figure 6C and D). Distinct walls were not easily distinguished in thin section due to the smaller size of structures and the very dark, micritic background.

Chemical analyses and X-ray Spectra of Walled Structures and Clay Fraction of Macerates

The minerals coating structures from both the Taishir and Kaknotwe formations were embedded in a carbonaceous matrix, as shown by the presence of a D-band at ~1320 to ~1360 cm^{-1} and a G-band at ~1590 cm^{-1} in the Raman spectra of the structures (e.g., McNeil *et al.*, 2015) (Figure 7). This demonstrates a close association of the minerals in the walls with an organic matrix.

EDS spectra of mineral grains on the surfaces of all structures from all formations contained peaks of Si, O, Al, K, Mg and Fe (Figure 8), suggesting the presence of clay minerals. Rare points (about 10%) on samples from the Kakontwe Formation also contained Ca and P peaks. About 10% of all examined points from the Rasthof Formation also contained trace amounts of Ti. Fewer than 10% of the 6 to 13 points examined per specimen contained only Si and O, indicating the presence of quartz.

Structures from different localities had similar compositions, although the surfaces of some structures contained several areas of concentrated iron oxide (areas identified under reflected light as red spots). Overall, chemical analyses indicated that putative microfossils contained a suite of minerals rather than a single mineral. The interiors and exteriors of putative microfossils produced identical EDS spectra (Figure 8), indicating that the various mineral grains preserved in these structures did not precipitate around or simply adsorb onto an original structure of different composition.

We compared the mineralogy of the walled structures and the fine size fraction of the bulk residues (< 0.2 μm) by X-ray diffraction to better understand the similarities and differences between clay mineral composition of the walled structures and mineralogy of the sediments in which the structures were preserved. Structures from the Kakontwe Formation contained quartz,

iron oxides, titanium oxides and mica group clay minerals (especially muscovite, Figure 9A). Also present was potassium-rich feldspar (microcline, Figure 9A). The clay size fraction from macerates also contained muscovite, quartz, iron and titanium oxides, and a small amount of microcline as well as additional peaks of dolomite (Figure 9A). Similarly, structures from the Taishir Formation contained quartz and some iron and titanium oxides, although the dominant clay mineral in these samples was illite rather than muscovite. These minerals were consistent with minerals peaks present in the XRD spectra of the fine size fraction of the residue from the Taishir Formation (Figure 9B).

Minerals in putative microfossils and the clay fraction from the Rasthof Formation were similar to those in the Kakontwe Formation, and included quartz, mica-group clay minerals (muscovite), and small amounts of iron and titanium oxides (Figure 9C). Also present in residue from the Rasthof Formation was a small amount of dolomite. Thus, in all three formations, putative microfossils were composed of a suite of minerals associated with a carbonaceous matrix, with the same compositions on the internal and external surfaces of structures. The mineralogy of putative microfossils was the same as the clay fraction of the corresponding residues at all three localities, showing an abundance of quartz and hydrous, potassium-rich aluminosilicates (either in the form of muscovite or illite), and small amounts of titanium and iron oxides. This striking similarity in mineral composition across these basins may be indicative of common biological or diagenetic processes that preserve the structures.

DISCUSSION

Biological Origin of Walled Structures

Several characteristics indicate a eukaryotic origin for the structures described in this study and distinguish them from transported coated grains that accumulated a siliceous or an aluminosilicate veneer. First, previous petrographic analyses of the Rasthof Formation displayed a close relationship between the walled structures and microbial textures, and lack evidence of strong traction currents needed to deliver coated grains to the microbialites (Figure 6, Pruss *et al.,* 2010; Bosak *et al.,* 2011; Dalton *et al.,* 2013; Bosak *et al.*, 2014). Microbial structures that form in high flow regimes have characteristic roughness and distributions with respect to the flow direction (Bosak *et al.,* 2013; Mariotti *et al.*, 2013; 2014), but none of these were apparent in the planar nature of analyzed microbial facies of the Rasthof and Kakontwe formations. Secondly, the walled structures also occur in unlaminated limestones of the Kakontwe and Taishir formations (Figure 6C), which lack additional similarly-sized grains. Thus, the structures must have grown and accumulated minerals *in situ*.

Similarities between the previously described fossils of testate eukaryotes from the Rasthof and Taishir formations (Bosak et al., 2011a, 2012; Dalton et al., 2013) and the newly discovered structures from the Kakontwe and Taishir formations indicate that the latter are also fossils of testate organisms. Structures from all three localities (Namibia, Zambia, and Mongolia), are hollow and have similar uniformly thick, carbonaceous and mineral-rich walls (Figures 2H, 4H, 5F, 6A and B)(Bosak et al., 2011a, 2012; Dalton et al., 2013). Compositionally and morphologically these walls are also similar to those of some modern testate organisms (Lahr and Lopes, 2006; Gooday et al., 2008, 2013; Ohkawara et al., 2009; Vohník et al., 2009; Šatkauskienė, 2014; Armynot du Châtelet et al., 2015; Rodrigues et al., 2015). Furthermore, the presence of carbonaceous matter in the walls of the microfossils (Figure 8), distinct morphological features (Figure 2, 4, 5), normal size or slightly skewed distributions (Figure 3)

and the narrow size ranges of the structures are consistent with those of microfossils assemblages (e.g., see distributions of body sizes of plankton by Clauset and Erwin, 2008, and late Quaternary mammals by Schmidt et al., 2006) rather than coated grains (e.g., see distributions of ooid sizes reported by Rankey *et al.*, 2006).

Mechanisms of Testate Fossil Preservation in Cap Carbonates

Previous studies interpreted the organic- and mineral-rich walls of structures from the Rasthof and the Taishir formations as products of biological selection of minerals by agglutinating microbial eukaryotes (Bosak *et al.*, 2011a; Dalton *et al.*, 2013). Here we evaluate the agglutination hypothesis and consider an alternative hypothesis. Specifically, the ubiquitous occurrence of clay minerals in test walls from three different paleocontinents may indicate that similar early diagenetic processes preserved the test walls during the deposition of cap carbonates. The latter hypothesis envisions the adsorption or precipitation of aluminosilicate minerals around the originally organic or siliceous test walls in solutions that otherwise favored extensive carbonate precipitation (Figure 10A).

Clay minerals have been suggested to play a key role in preservation of organic matter, with several studies showing a close association between siliciclastic minerals and microbial organisms (Wacey et al., 2014; McMahon et al., 2016; Newman et al., 2016). Newman et al. (2016) demonstrated through experimental preservation of cyanobacterial mats the potential for clay minerals in suspension to coat bacterial filaments and promote preservation. It has been additionally suggested that the inhibition of growth due to clay mineral coating promotes preservation of soft tissue in bacteria (McMahon et al., 2016). In these cases, the clay minerals coating the organic matter are more taphonomically robust than the soft material and would

therefore likely be preserved in the rock record. In contrast, Wacey et al. (2014) describe fossils of organic walled microfossils from the Torridon Group of Scotland which they argue represent authigenic clay preservation based on the zonation of minerals and lack of detrital textures. While these studies focus on filamentous bacteria and do not resemble the sizes and morphologies of microfossils described here, the textures and distributions of clay minerals described by Newman et al (2016) and McMahon et al. (2016) are similar to those of microfossils from the Kakontwe, Taishir and Rasthof formations, which lack zonation and smooth textures described by Wacey et al. (2014). This suggests that coating of clay minerals rather than precipitation of authigenic clays more likely played a role in fossil preservation in the Kakontwe, Taishir and Rasthof formations.

Michalopoulos *et al.* (2000) demonstrated the transformation of biogenic silica in diatom frustules into authigenic clays in Amazon deltaic deposits. Similar mineral replacement of amorphous silica around diatoms by clay minerals was reported in saline lakes in Bolivia, where smectite precipitates in sheets over the siliceous frustules (Badaut and Risacher, 1983). In both cases, some remnants of the original biogenic siliceous structure remain, and the precipitation of clays requires the presence of localized sources of amorphous silica (diatom frustules) as well as sources of aluminum. While these requirements are consistent with the reported occurrence of the processes in siliciclastic sediments, they are inconsistent with the carbonate-precipitating environments in which the Kakontwe, Taishir, and Rasthof formations would have been deposited.

If similar processes played a role in formation of minerals around microfossils from the Kakontwe, Taishir and Rasthof formations, originally siliceous tests would be converted to clay-rich structures by authigenic aluminosilicate minerals after the death and burial of walled

organisms (Figure 10A). However, microfossils from post-Sturtian cap carbonates show no difference in mineral composition between internal and external surfaces of walls (Figure 8), do not preserve remnants of any original siliceous structures (Figures 2, 4, and 5), are comprised of a suite of individual clay mineral grains, and contain minerals such as TiO_2 and K-feldspar that do not form by authigenic processes. Furthermore, the individual mineral grains that make up the walled microfossils from the Kakontwe, Taishir, and Rasthof formations (Figures 2, 4, and 5) are texturally different from the continuous and relatively smooth authigenic clays that surround diatom frustules (e.g., Badaut and Risacher, 1983). Instead, the mineralogy of microfossils from the Taishir, Kakontwe and Rasthof formations is consistent with modern examples of agglutinating testate organisms.

The mineral composition and sizes of grains in microfossils from the Taishir, Kakontwe and Rasthof formations, while offering little evidence to support formation of authigenic minerals around siliceous or organic rich walls, are consistent with those of modern agglutinating testate organisms. Modern examples of agglutinating microbes actively collect and select for specific types of mineral grains from the sediment and cement them together with silica, calcite or organic cements (Nikolaev *et al.*, 2005; Vohník *et al.*, 2009; Armynot du Châtelet *et al.*, 2010; Šatkauskienė, 2014; Sabatini *et al.*, 2016). These organomineral associations have a high preservation potential because they retain both detrital grains and the organic component, and acquire a stronger signal of diagenetic quartz over time (McNeil et al., 2015). Microfossils from these localities may therefore represent agglutinated tests that preserve the original structure and mineralogy of tests after burial (Figure 10B). Modern agglutinating microbial eukaryotes select for calcareous or siliceous minerals. Some of these are flat, micaceous grains with uniform sizes within a given organism (Armynot du Châtelet et al., 2010; Šatkauskienė, 2014). In fact, some

modern lobose amoebae and foraminifera select for minerals that comprise only a small fraction of the bulk sediment, and may concentrate minerals such as zircons, ilmenite and titanium (Armynot du Châtelet et al., 2010, 2015; Makled and Langer, 2010; Sabbatini et al., 2016). The large concentrations of minerals in tests relative to the surrounding micrite or the microbial laminae (c.f., Fig 3 in Bosak et al., 2011a; Newman et al., 2016) also favors active, composition- and size-selective biological agglutination over passive trapping by the exopolymeric substances in the surrounding microbial laminae or presumably sticky eukaryotic surfaces. Thus size distributions and shapes of mineral grains in microfossils as well as mineral composition of tests relative to sediments are consistent with selective and active agglutination of tests by eukaryotic organisms.

Microfossils from all three localities contain a suite of mineral grains between 5 μm and 20 μm across and include quartz, clay minerals (illite and muscovite) and occasional iron and titanium oxides (Figure 9). These minerals are also present in the fine size fraction of the residues and include distinctly non-authigenic components such as TiO_2 and K-feldspar. This fraction may have been delivered to the carbonate-precipitating marine environments as the wind-blown or fine-grained component of distal riverine input (e.g., Muhs et al., 2001; Prospero, 1972). These minerals, then, would have been present in sediments along with carbonate minerals, making them available to test-building organisms. The difference in dominant clay minerals between the Taishir Formation and the Kakontwe and Rasthof formations may be due to the higher metamorphic grade of the latter formations, which can result in conversion of illite to muscovite (Totten and Blatt, 1996; Verdel et al., 2011). Thus, microfossils from all three formations were likely initially composed of similar minerals. Such striking consistency in mineralogy between the three localities, therefore, likely indicates similar selectivity in mineral

type and size by organisms during agglutination rather than identical diagenetic processes affecting altering the microfossil assemblages from three geographically distinct localities.

Possible Taxonomic Affinities

Several groups of modern test-forming microbial eukaryotes, including testate amoebae and foraminifera, are known to have similar sizes, morphologies and test compositions to microfossils from the Kakontwe, Taishir and Rasthof formations. The size ranges and normal distributions of fossil tests from the Kakontwe Formation (90 +/- 5 μm – 200 +/- 5 μm, N=100), the Taishir Formation (50 +/- 5 μm – 140 +/- 5 μm, N=50), and the Rasthof Formation (80 μm – 218 μm, N=114; Dalton et al., 2013) are consistent with modern lobose testate amoebae (~30 μm to ~300 μm, Lahr and Lopes, 2009) and agglutinated foraminifera such as saccamminids and psammosphaerids (<100 μm to >125 μm, Gooday et al., 2013; Ohkawara et al., 2009).

Microfossils from the Kakontwe, Taishir and Rasthof formations have very simple spherical and ovoid morphologies, but lack some of the more diagnostic characteristics described previously in tests from the Ongongo and the Okaaru localities of the Rasthof Formation (Bosak et al., 2011a, 2012; Dalton et al., 2013), including hoods, curved necks and asymmetrically positioned slits or apertures that would strengthen the case for their similarity to lobose testate amoebae. The most distinguishing features of tests described here include blunt or curved edges or tear shapes. Indeed, round, spherical, ovoid, and tear-shaped morphologies are present in some modern lobose testate amoebae, including species of the group Arcellinida (Amoebazoa) such as Heleoperidae, Plagiopyxidae, and Difflugidae (Vohník *et al.,* 2009; Bosak *et al.,* 2011; Gomaa *et al.,* 2012; Lahr & Lopes 2006; Lahr & Lopes 2009; Gomaa *et al.,* 2012) as well as in some modern agglutinating foraminifera, such as saccamminids and psammosphaerids (Ohkawara *et*

al., 2009; Gooday *et al.,* 2008; Gooday *et al.,* 2013; Rodrigues *et al.,* 2015; Sabbatini *et al.*, 2016). A new morphology is also present in these microfossil assemblages: round structures with concave edges, which suggest intentional formation by an organism. Although there are no modern examples of testate organisms with such features, they expand the morphological and, by inference, morphospecies diversity of agglutinated testate eukaryotes in post-Sturtian cap carbonates.

Paleoecology

The commonality of fossils of testate eukaryotes in cap carbonates from the Kakontwe, Rasthof and Taishir formations suggests that eukaryotic organisms were abundant and globally distributed in the aftermath of the Sturtian glaciation. The compositional and broad morphological similarities across the three basins demonstrate that similar classes of organisms were selectively preserved during the deposition of cap carbonates. The close association of these organisms with microbially laminated sediments in both the Kakontwe and the Rasthof formations indicates that the testate organisms were likely benthic, a life style consistent with the formation of tests by agglutination. In contrast to a recent study of 5 Sturtian glacial and interglacial shales, which preserve mostly organic-walled fossils of planktonic prokaryotes (Riedman et al., 2014), our study finds abundant fossils of benthic eukaryotic organism in shallow carbonate-depositing environments. This emphasizes the key role of cap carbonates in assessing eukaryotic lifestyles and diversity after the Sturtian glaciation. Evidence of morphospecies diversity among these organisms and across different basins comes from the variation of test sizes and specific morphological features like concave edges. Additionally, differences in relative proportions of ovoid, spherical and other morphologies in different

formations and even in different parts of the same formations (e.g., Dalton *et al.*, 2013) reinforce the inferences of diversity within and among microbial assemblages. This morphospecies diversity, found in cap carbonates, is greater than the diversity of organic fossils previously described in shale deposits (Riedman et al., 2014). These shale deposits preserve at least 10 different morphospecies, but the majority of microfossils are representative of bacteria with few examples of confidently assigned eukaryotes (Riedman et al., 2014). Microfossils of the Kakontwe, Taishir and Rasthof formations, on the other hand, contain at least six distinct morphologies (ovoid, spherical, tapered, ovoid with blunt or concave edges, spherical with blunt or concave edges, and ovoid with possible hoods), suggesting that diverse morphospecies of eukaryotes were present in the nonglacial interlude. Therefore, our study provides new insights by investigating a different depositional environment with a distinct set of ecological and preservational conditions. Future studies of other cap carbonates are likely to further increase the observed fossil diversity in Neoproterozoic post-glacial deposits.

CONCLUSIONS

This study identifies abundant structures with mineral- and organic-rich walls in previously unexamined samples of post-Sturtian cap carbonate deposits from the Kakontwe and Taishir formations. The new structures from the Kakontwe and Taishir formations are similar to those reported from the Rasthof Formation (Bosak et al., 2011; Dalton et al., 2013) and are interpreted as fossil tests of agglutinated microbial eukaryotes. The microfossils exhibit both morphological and compositional similarities across basins and expand the morphological diversity of agglutinated organisms preserved in cap carbonates. The new findings strengthen the case for test-building by agglutination and indicate that similar types of microbial eukaryotes

were distributed globally and were widely preserved during the deposition of cap carbonates. The presence of similar, agglutinating organisms in three distinct geographic basins examined to date suggests that microbial eukaryotic communities thrived in the greenhouse aftermath of the Sturtian glaciations.

ACKNOWLEDGEMENTS

We acknowledge the Smith College Tomlinson Fund, the Smith College Geosciences Department, and the MIT NAI node for funding of this project. This work made use of the Shared Experimental Facilities supported in part by the MRSEC Program of the National Science Foundation under award number DMR -1419807. We thank J. Wopereis, J. Brady, M. Vollinger, and A. McClelland for assistance with sample preparation and analyses, R. Newton for insights and helpful conversations, and M. Abedinejad and D. Kortes for technical support.

REFERENCES

ARMYNOT DU CHÂTELET, E., BERNARD, N., DELAINE, M., POTDEVIN, J.L., and GILBERT, D., 2015, The mineral composition of the tests of "testate amoebae" (Amoebozoa, Arcellinida): The relative importance of grain availability and grain selection: Revue de Micropaleontologie, v. 58, p. 141–154, doi: 10.1016/j.revmic.2015.05.001. http://dx.doi.org/10.1016/j.revmic.2015.05.001.

ARMYNOT DU CHÂTELET, E., GUILLOT, F., RECOURT, P., VENTALON, S., and TRIBOVILLARD, N., 2010, Influence of sediment grain size and mineralogy on testate amoebae test construction: Comptes Rendus Geoscience, v. 342, p. 710–717, doi: 10.1016/j.crte.2010.05.002. http://www.sciencedirect.com/science/article/pii/S1631071310001562.

BADAUT, D., and RISACHER, F., 1983, Authigenic smectite on diatom frustules in Bolivian saline lakes: Geochimica et Cosmochimica Acta, v. 47, p. 363–375.

BATUMIKE, M.J., CAILTEUX, J.L.H., and KAMPUNZU, A.B., 2007, Lithostratigraphy, basin development, base metal deposits, and regional correlations of the Neoproterozoic Nguba and Kundelungu rock successions, central African Copperbelt: Gondwana Research, v. 11, p. 432–447, doi: 10.1016/j.gr.2006.04.012.

BODISELITSCH, B., KOEBERL, C., MASTER, S., and REIMOLD, W.U., 2005, Estimating duration and intensity of Neoproterozoic Snowball glaciations from Ir anomalies: Science, v. 308, p. 239–242, doi: 10.1126/science.1104657.

http://www.sciencemag.org/cgi/doi/10.1126/science.1104657.
BOLD, U., SMITH, E.F., ROONEY, A.D., BOWRING, S.A., BUCHWALDT, R., DUDAS, F.O., RAMEZANI, J., CROWLEY, J.L., SCHRAG, D.P., and MACDONALD, F.A., 2016, Neoproterozoic stratigraphy of the zavkhan terrane of Mongolia: The backbone for cryogenian and early ediacaran chemostratigraphic records: American Journal of Science, v. 315, p. 1–63, doi: 10.2475/01.2016.01.
BOSAK, T., LAHR, D.J.G., PRUSS, S.B., MACDONALD, F.A., DALTON, L., and MATYS, E., 2011a, Agglutinated tests in post-Sturtian cap carbonates of Namibia and Mongolia: Earth and Planetary Science Letters, v. 308, p. 29–40, doi: 10.1016/j.epsl.2011.05.030. http://dx.doi.org/10.1016/j.epsl.2011.05.030.
BOSAK, T., LAHR, D.J.G., PRUSS, S.B., MACDONALD, F.A., GOODAY, A.J., DALTON, L., and MATYS, E.D., 2012, Possible early foraminiferans in post-sturtian (716-635 Ma) cap carbonates: Geology, v. 40, p. 67–70, doi: 10.1130/G32535.1.
BOSAK, T., MACDONALD, F., LAHR, D., and MATYS, E., 2011b, Putative Cryogenian ciliates from Mongolia: Geology, v. 39, p. 1123–1126, doi: 10.1130/G32384.1.
BOSAK, T., MARIOTTI, G., MACDONALD, F., PERRON, T., and PRUSS, S., 2013, Microbial sedimentology of stromatolites in Neoproterozoic cap carbonates: The Paleontological Society Papers, v. 19, p. 1–25. http://web.mit.edu/perron/www/files/Bosak13.pdf.
BUTTERFIELD, N.J., 2000, Bangiomorpha pubescens n. gen., n. sp.: implications for the evolution of sex, multicellularity, and the Mesoproterozoic/Neoproterozoic radiation of eukaryotes: Paleobiology, v. 26, p. 386–404, doi: 10.1666/0094-8373(2000)026<0386:bpngns>2.0.co;2. http://paleobiol.geoscienceworld.org/content/26/3/386.abstract.
BUTTERFIELD, N.J., and RAINBIRD, R.H., 1998, Diverse organic-walled fossils, including "possible dinoflagellates," from the early Neoproterozoic of arctic Canada: Geology, v. 26, p. 963–966, doi: 10.1130/0091-7613(1998)026<0963:DOWFIP>2.3.CO;2.
CLAUSET, A., and ERWIN, D.H., 2008, The evolution and distribution of species body size: Science, v. 321, p. 399–401, doi: 10.1126/science.1157534.
COHEN, P.A., and MACDONALD, F.A., 2015, The Proterozoic record of eukaryotes: Paleobiology, v. 41, p. 1–23, doi: 10.1017/pab.2015.25. http://www.journals.cambridge.org/abstract_S0094837315000251.
CORSETTI, F.A., AWRAMIK, S.M., and PIERCE, D., 2003, A complex microbiota from from snowball Earth times: Microfossils from the Neoproterozoic Kingston Peak Formation, Death Valley, USA: PNAS, v. 100, p. 4399–4404.
COSTAS, E., FLORES-MOYA, A., and LÓPEZ-RODAS, V., 2008, Rapid adaptation of phytoplankters to geothermal waters is achieved by single mutations: were extreme environments "Noah"s Arks' for photosynthesizers during the Neoproterozoic "snowball Earth"? New Phytologist, v. 180, p. 922–932, doi: 10.1111/j.1469-8137.2008.02620.x.
DALTON, L.A., BOSAK, T., MACDONALD, F.A., LAHR, D.J.G., and PRUSS, S.B., 2013, Preservational and morphological variability of assemblages of agglutinated eukaryotes in Cryogenian cap carbonates of northern Namibia: Palaios, v. 28, p. 67–79, doi: 10.2110/palo.2012.p12-084r. http://palaios.sepmonline.org/cgi/doi/10.2110/palo.2012.p12-084r.
GOMAA, F., TODOROV, M., HEGER, T.J., MITCHELL, E.A.D., and LARA, E., 2012, SSU rRNA Phylogeny of Arcellinida (Amoebozoa) reveals that the largest Arcellinid genus, Difflugia leclerc 1815, is not monophyletic: Protist, v. 163, p. 389–399, doi: 10.1016/j.protis.2011.12.001.

GOODAY, A.J., KAMENSKAYA, O.E., and SOLTWEDEL, T., 2013, Basal foraminifera and gromiids (Protista) at the Håkon-Mosby Mud Volcano (Barents Sea slope): Marine Biodiversity, v. 43, p. 205–225, doi: 10.1007/s12526-013-0148-5.

GOODAY, A.J., NOMAKI, H., and KITAZATO, H., 2008, Modern deep-sea benthic foraminifera: a brief review of their morphology-based biodiversity and trophic diversity: Geological Society, London, Special Publications, v. 303, p. 97–119, doi: 10.1144/SP303.8. http://sp.lyellcollection.org/content/303/1/97.abstract.

HOFFMAN, P.F., MACDONALD, F. a., and HALVERSON, G.P., 2011, Chemical sediments associated with Neoproterozoic glaciation: iron formation, cap carbonate, barite and phosphorite: Geological Society, London, Memoirs, v. 36, p. 67–80, doi: 10.1144/M36.5.

HOFFMAN, P.F., and SCHRAG, D.P., 2002, The snowball Earth hypothesis: testing the limits of global change: Terra, v. 14, p. 129–155, doi: 10.1080/713604466. http://onlinelibrary.wiley.com/doi/10.1046/j.1365-3121.2002.00408.x/full.

JOHNSTON, D.T., MACDONALD, F. a., GILL, B.C., HOFFMAN, P.F., and SCHRAG, D.P., 2012, Uncovering the Neoproterozoic carbon cycle: Nature, v. 483, p. 320–323, doi: 10.1038/nature10854. http://dx.doi.org/10.1038/nature10854.

KNOLL, a H., 1992, The early evolution of eukaryotes: a geological perspective.: Science, v. 256, p. 622–627, doi: 10.1126/science.1585174.

LAHR, D.J.G., and LOPES, S.G.B.C., 2009, Evaluating the taxonomic identity in four species of the lobose testate amoebae genus Arcella Ehrenberg, 1832: Acta Protozoologica, v. 48, p. 127–142.

LAHR, D.J.G., and LOPES, S.G.B.C., 2006, Morphology, biometry, ecology and biogeography of five species of Difflugia Leclerc, 1815 (Arcellinida: Difflugiidae), from Tiete River, Brazil: Acta Protozoologica, v. 45, p. 77–90.

LIU, Y., and PELTIER, W.R., 2010, A carbon cycle coupled climate model of Neoproterozoic glaciation: Influence of continental configuration on the formation of a "soft snowball": Journal of Geophysical Research Atmospheres, v. 115, p. 1–19, doi: 10.1029/2009JD013082.

MACDONALD, F.A., JONES, D.S., and SCHRAG, D.P., 2009, Stratigraphic and tectonic implications of a newly discovered glacial diamictite-cap carbonate couplet in southwestern Mongolia: Geology, v. 37, p. 123–126, doi: 10.1130/G24797A.1.

MAKLED, W.A., and LANGER, M.R., 2010, Preferential selection of titanium-bearing minerals in agglutinated Foraminifera: Ilmenite (FeTiO3) in Textularia hauerii d'Orbigny from the Bazaruto Archipelago, Mozambique: Revue de Micropaléontologie, v. 53, p. 163–173, doi: 10.1016/j.revmic.2009.11.001. http://www.sciencedirect.com/science/article/pii/S0035159809000506.

MASTER, S., and WENDORFF, M., 2011, Neoproterozoic glaciogenic diamictites of the Katanga Supergroup, Central Africa: The Geological Record of Neoproterozoic Glaciations. Geological Society, London, Memoirs, v. 36, p. 173–184, doi: 10.1144/M36.12. http://mem.lyellcollection.org/cgi/doi/10.1144/M36.12.

MCMAHON, S., ANDERSON, R.P., SAUPE, E.E., and BRIGGS, D.E.G., 2016, Experimental evidence that clay inhibits bacterial decomposers: Implications for preservation of organic fossils: Geology, v. 44, p. G38454.1, doi: 10.1130/G38454.1. http://geology.gsapubs.org/lookup/doi/10.1130/G38454.1.

MCNEIL, D.H., SCHULZE, H.G., MATYS, E., and BOSAK, T., 2015, Raman spectroscopic analysis of carbonaceous matter and silica in the test walls of recent and fossil agglutinated

foraminifera: AAPG Bulletin, v. 99, p. 1081–1097, doi: 10.1306/12191414093.
MICHALOPOULOS, P., ALLER, R.C., and REEDER, R.J., 2000, Conversion of diatoms to clays during early diagenesis in tropical, continental shell muds: Geology, v. 28, p. 1095–1098, doi: 10.1130/0091-7613(2000)28<1095:CODTCD>2.0.CO.
MUHS, D.R., BETTIS, E. a., BEEN, J., and MCGEEHIN, J.P., 2001, Impact of Climate and Parent Material on Chemical Weathering in Loess-derived Soils of the Mississippi River Valley: Soil Science Society of America Journal, v. 65, p. 1761, doi: 10.2136/sssaj2001.1761.
NEWMAN, S.A., MARIOTTI, G., PRUSS, S., and BOSAK, T., 2016, Insights into cyanobacterial fossilization in Ediacaran siliciclastic environments: Geology, v. 44, p. 579–582, doi: 10.1130/G37791.1.
NIKOLAEV, S.I., MITCHELL, E.A.D., PETROV, N.B., BERNEY, C., FAHRNI, J., and PAWLOWSKI, J., 2005, The testate lobose amoebae (order Arcellinida Kent, 1880) finally find their home within Amoebozoa: Protist, v. 156, p. 191–202, doi: 10.1016/j.protis.2005.03.002.
OHKAWARA, N., KITAZATO, H., UEMATSU, K., and GOODAY, A.J., 2009, A minute new species of Saccammina (monothalamous Foraminifera; Protista) from the abyssal Pacific: Journal of Micropalaeontology, v. 28, p. 143–151, doi: 10.1144/jm.28.2.143. <Go to ISI>://000275314600005.
PROSPERO, J.M., 1972, Vertical and areal distribution of Saharan dust over the Western Equatorial North Atlantic Ocean: Journal of Geophysical Research, v. 77, p. 5255–5265.
PRUSS, S.B., BOSAK, T., MACDONALD, F.A., MCLANE, M., and HOFFMAN, P.F., 2010, Microbial facies in a Sturtian cap carbonate, the Rasthof Formation, Otavi Group, northern Namibia: Precambrian Research, v. 181, p. 187–198, doi: 10.1016/j.precamres.2010.06.006. http://dx.doi.org/10.1016/j.precamres.2010.06.006.
RIEDMAN, L.A., PORTER, S.M., HALVERSON, G.P., HURTGEN, M.T., and JUNIUM, C.K., 2014, Organic-walled microfossil assemblages from glacial and interglacial Neoproterozoic units of Australia and Svalbard: Geology, v. 42, p. 1011–1014, doi: 10.1130/G35901.1.
RODRIGUES, A., DE SANTIS BRAGA, E., and EICHLER, B.B., 2015, Living foraminifera in the shallow waters of Admiralty Bay: distributions and environmental factors: Journal of Foraminiferal Research, v. 45, p. 128–145.
ROONEY, A.D., STRAUSS, J. V., BRANDON, A.D., and MACDONALD, F.A., 2015, A Cryogenian chronology: Two long-lasting synchronous neoproterozoic glaciations: Geology, v. 43, p. 459–462, doi: 10.1130/G36511.1.
SABBATINI, A., NEGRI, A., BARTOLINI, A., MORIGI, C., BOUDOUMA, O., DINELLI, E., FLORINDO, F., GALEAZZI, R., HOLZMANN, M., LURCOCK, P.C., MASSACCESI, L., PAWLOWSKI, J., and ROCCHI, S., 2016, Selective zircon accumulation in a new benthic foraminifer, *Psammophaga zirconia* , sp. nov.: Geobiology, p. n/a–n/a, doi: 10.1111/gbi.12179. http://doi.wiley.com/10.1111/gbi.12179.
ŠATKAUSKIENĖ, I., 2014, Testate amoebae (Testaceae) of Lithuania: Biologija, v. 60, p. 59–69.
SCHMIDT, D.N., LAZARUS, D., YOUNG, J.R., and KUCERA, M., 2006, Biogeography and evolution of body size in marine plankton: Earth-Science Reviews, v. 78, p. 239–266, doi: 10.1016/j.earscirev.2006.05.004.
SHIELDS, G., and VEIZER, J., 2002, The Precambrian marine carbonate isotope database: version 1.1.: Geochemistry Geophysics Geosystems, v. 3, p. 1 – 12, doi: 10.1029/2001GC000266. http://discovery.ucl.ac.uk/43794/.
TOTTEN, M.W., and BLATT, H., 1996, Sources of silica from the illite to muscovite transformation during late-stage diagenesis of shales: SEPM, p. 85–92.

TZIPERMAN, E., ABBOT, D.S., ASHKENAZY, Y., GILDOR, H., POLLARD, D., SCHOOF, C.G., and SCHRAG, D.P., 2012, Continental constriction and oceanic ice-cover thickness in a Snowball-Earth scenario: Journal of Geophysical Research: Oceans, v. 117, p. 1–12, doi: 10.1029/2011JC007730.

VERDEL, C., NIEMI, N., and VAN DER PLUIJM, B. a., 2011, Variations in the illite to muscovite transition related to metamorphic conditions and detrital muscovite content: Insight from the Paleozoic passive margin of the southwestern United States: The Journal of Geology, v. 119, p. 419–437, doi: 10.1086/660086.

VOHNÍK, M., BURDÍKOVÁ, Z., ALBRECHTOVÁ, J., and VOSÁTKA, M., 2009, Testate amoebae (Arcellinida and Euglyphida) vs. Ericoid mycorrhizal and DSE fungi: A possible novel interaction in the mycorrhizosphere of ericaceous plants? Microbial Ecology, v. 57, p. 203–214, doi: 10.1007/s00248-008-9402-y.

WACEY, D., SAUNDERS, M., ROBERTS, M., MENON, S., GREEN, L., KONG, C., CULWICK, T., STROTHER, P., and BRASIER, M.D., 2014, Enhanced cellular preservation by clay minerals in 1 billion-year-old lakes.: Scientific reports, v. 4, p. 5841, doi: 10.1038/srep05841. http://www.ncbi.nlm.nih.gov/pubmed/25068404.

WENDORFF, M., and KEY, R.M., 2009, The relevance of the sedimentary history of the Grand Conglomerat Formation (Central Africa) to the interpretation of the climate during a major Cryogenian glacial event: Precambrian Research, v. 172, p. 127–142, doi: 10.1016/j.precamres.2009.03.013.

FIGURE CAPTIONS

Table 1: List of all examined of samples from the Kakontwe, Taishir and Rasthof formations. Samples are housed at Smith College in Northampton, MA.

Figure 1: Stratigraphic columns of the Tsagaan Olom Group of the Zavkhan Terrane, Mongolia (a) and the Katangan Supergroup of the Kipushi Basin, Zambia (b). Columns show the stratigraphic location of the Taishir Formation (a) and the Kakontwe Formation (b) with the location of samples and microfossil occurrence.

Figure 2: SEM images of putative microfossils from the Kakontwe Formation. Structures demonstrate ovoid morphologies that taper along the long axis to create a tear shape (a), ovoid tapering morphologies with possible openings shown by a white arrow (b), spherical morphologies with blunt (c) or concave (d) edges (highlighted by a white arrow), ovoid morphologies with possible opening along the smaller axis shown by a white arrow, ovoid morphologies with blunt edges (f), ovoid morphologies with possible breaks shown by an arrow (g), and broken specimens demonstrating a hollow interior with 10 +/- 1 μm thick walls (h).

Figure 3: Size distributions of the long and short axes of putative microfossils the Kakontwe and Taishir formations. Structures of the Kakontwe Formation and the Taishir Formation both demonstrate a normal distribution. Structures from the Kakontwe Formation have slightly larger sizes than those of the Taishir Formation, though the ranges for the two formations have clear overlap.

Figure 4: SEM images of characteristic structures from the Taishir Formation. Structures are predominantly spherical with possible openings highlighted by white arrows (a, h), concave (b, c) or blunt (d, e) edges, possible elongated openings indicated by arrows (f, g), or tapering along the long axis (e). Structures are hollow and have 10 +/- 1 μm thick walls (h).

Figure 5: SEM images of putative microfossils from the Rasthof Formation. Structures show characteristic morphologies, including elongated ovoid forms (a), spherical forms with possible openings shown by a white arrow (b), ovoid forms with possible openings shown by arrows (b, d), structures with hoods shown by an arrow (e), and broken forms showing a hollow interior with 10 +/- 1 μm thick walls (f).

Figure 6: Petrographic thin section images of samples from the Kakontwe (a, b) and Taishir (c, d) formations. Putative microfossils from the Kakontwe Formation are found in both massive (a) and microbially laminated (b) limestones. These structures are oval to circular in thin section and have a distinct outer wall with micritic filling. Putative microfossils from the Taishir Formation are found in unlaminated limestones and are circular in thin section and infilled with dark micrite (c, d).

Figure 7: Raman spectrometry data showing peaks at ~1320 to 1360 cm^{-1} and ~1590 cm^{-1} characteristic of carbonaceous material in the walls of putative microfossils.

Figure 8: EDS data showing the elemental compositions of the interior and exterior surfaces of microfossils. Au and Pd peaks are the result of gold and palladium coating used on samples to enhance conductivity and are not originally present in samples.

Figure 9: XRD spectra showing mineralogy of putative microfossils (blue) and residues (red) from the Kakontwe (a), Taishir (b), and Rasthof (c) formations. Residues and putative microfossils from all three localities have the same composition and contain illite or muscovite as the major clay mineral.

Figure 10: Cartoon depictions of possible preservation models for microfossils of the Kakontwe, Taishir, and Kakontwe formations. Model “a” depicts diagenetic alteration through adsorption or precipitation of clay minerals to an originally siliceous or organic walled test. Model “b” illustrates preservation of an originally agglutinated test.

Supplemental Figure 1: A locality map showing the locations of the Kakontwe Formation, the Rasthof Formation, and the putative location of the Taishir Formation during the Cyrogenian.

Supplemental Figure 2: EDS point analysis spectra from a representative microfossil of the Kakontwe Formation. These spectra demonstrate the presence of aluminosilicate minerals as well as iron oxides and some calcium and phosphorous rich minerals.

Locality	Formation	Sample Name	Microfossils	Morphology	Size (μm)	Test Appearance
Zambia	Kakontwe	K1-54.10	Abundant	Ovoid/Spherical	~90-200	Dark grey
Zambia	Kakontwe	K2-58.25	Abundant	Ovoid/Spherical	~90-200	White with red spots
Zambia	Kakontwe	K3-62.85	Abundant	Ovoid/Spherical	~90-200	Dark grey
Zambia	Kakontwe	K4-66.51	Abundant	Ovoid/Spherical	~90-200	Dark grey
Zambia	Kakontwe	K6-76.50	Abundant	Ovoid/Spherical	~90-200	Dark grey
Zambia	Kakontwe	K7-79.75	Present	Spherical	~90-200	Dark grey
Zambia	Kakontwe	K8-84.85	None	N/A	N/A	N/A
Zambia	Kakontwe	K9-91.53	Abundant	Ovoid/Spherical	~90-200	Dark grey
Zambia	Kakontwe	K11-102.46	Present	Ovoid/Spherical	~90-200	Dark grey
Zambia	Kakontwe	K12-107.02	Present	Spherical	~90-200	Dark grey
Zambia	Kakontwe	K13-111.70	Abundant	Ovoid/Spherical	~90-200	Dark grey
Zambia	Kakontwe	K14-115.00	Present	Ovoid/Spherical	~90-200	Dark grey
Zambia	Kakontwe	K16-126.03	Present	Ovoid/Spherical	~90-200	Dark grey
Zambia	Kakontwe	K17-130.55	Abundant	Ovoid/Spherical	~90-200	Dark grey
Zambia	Kakontwe	K18-134.36	Present	Spherical	~90-200	Dark grey
Zambia	Kakontwe	K19-136.91	Present	Spherical	~90-200	Dark grey
Zambia	Kakontwe	K20-137.93	None	N/A	N/A	N/A
Zambia	Kakontwe	K22-138.26	None	N/A	N/A	N/A
Zambia	Kakontwe	K24-138.56	None	N/A	N/A	N/A
Mongolia	Taishir	F1125-0.9	None	N/A	N/A	N/A
Mongolia	Taishir	F1125-2.3	None	N/A	N/A	N/A
Mongolia	Taishir	F1125-3.0	None	N/A	N/A	N/A
Mongolia	Taishir	F1125-4.0	None	N/A	N/A	N/A
Mongolia	Taishir	F1125-6.0	Abundant	Spherical	~50-140	Dark grey/olive green
Mongolia	Taishir	F1125-6.5	Abundant	Spherical	~50-140	Dark grey/black
Mongolia	Taishir	F1125-7.0	Abundant	Spherical	~50-140	Dark grey
Mongolia	Taishir	F1125-7.5	Abundant	Spherical	~50-140	Yellow and grey
Mongolia	Taishir	F1125-8.1	Abundant	Spherical	~50-140	Dark grey
Mongolia	Taishir	F1125-8.5	Abundant	Spherical	~50-140	Dark grey/black
Mongolia	Taishir	F1125-10.0	Abundant	Spherical	~50-140	White, yellow, grey
Mongolia	Taishir	F1125-10.5	Abundant	Spherical	~50-140	White, yellow, grey
Mongolia	Taishir	F1125-30.0	None	N/A	N/A	N/A
Mongolia	Taishir	F1125-31.7	None	N/A	N/A	N/A
Mongolia	Taishir	F1125-33.0	None	N/A	N/A	N/A
Mongolia	Taishir	F1125-34.6	None	N/A	N/A	N/A
Mongolia	Taishir	F1125-38.0	None	N/A	N/A	N/A
Mongolia	Taishir	F1125-42.0	None	N/A	N/A	N/A

Okaaru, Namibia	Rasthof	OK5A	Abundant	Ovoid	~50-120	White with red spots
Okaaru, Namibia	Rasthof	OK5B	Present	Ovoid	~50-120	White with red spots
Okaaru, Namibia	Rasthof	OK5C	Present	Ovoid/Spherical	~50-120	White with red spots
Okaaru, Namibia	Rasthof	OK5D	Abundant	Ovoid	~50-120	White with red spots
Okaaru, Namibia	Rasthof	OK5E	Present	Ovoid	~50-120	White with red spots
Okaaru, Namibia	Rasthof	OK6A	Present	Ovoid/Spherical	~50-120	White with red spots
Okaaru, Namibia	Rasthof	OK6B	Present	Ovoid/Spherical	~50-120	White with red spots
Okaaru, Namibia	Rasthof	OK6C	Present	Ovoid/Spherical	~50-120	White with red spots
Ongongo, Namibia	Rasthof	ON2R 134.0	Present	Ovoid	~50-120	White with red spots
Ongongo, Namibia	Rasthof	ON2R 142.0	Present	Ovoid/Spherical	~50-120	White with red spots
Ongongo, Namibia	Rasthof	P7500 90.0	None	N/A	N/A	N/A
Ongongo, Namibia	Rasthof	P7500 133.8	Present	Ovoid	~50-120	White with red spots
Ongongo, Namibia	Rasthof	P7500 140.0	None	N/A	N/A	N/A
Ongongo, Namibia	Rasthof	P7500 151.0	Present	Ovoid	~50-120	White with red spots
Ongongo, Namibia	Rasthof	ON2R3B	Present	Ovoid	~50-120	White with red spots

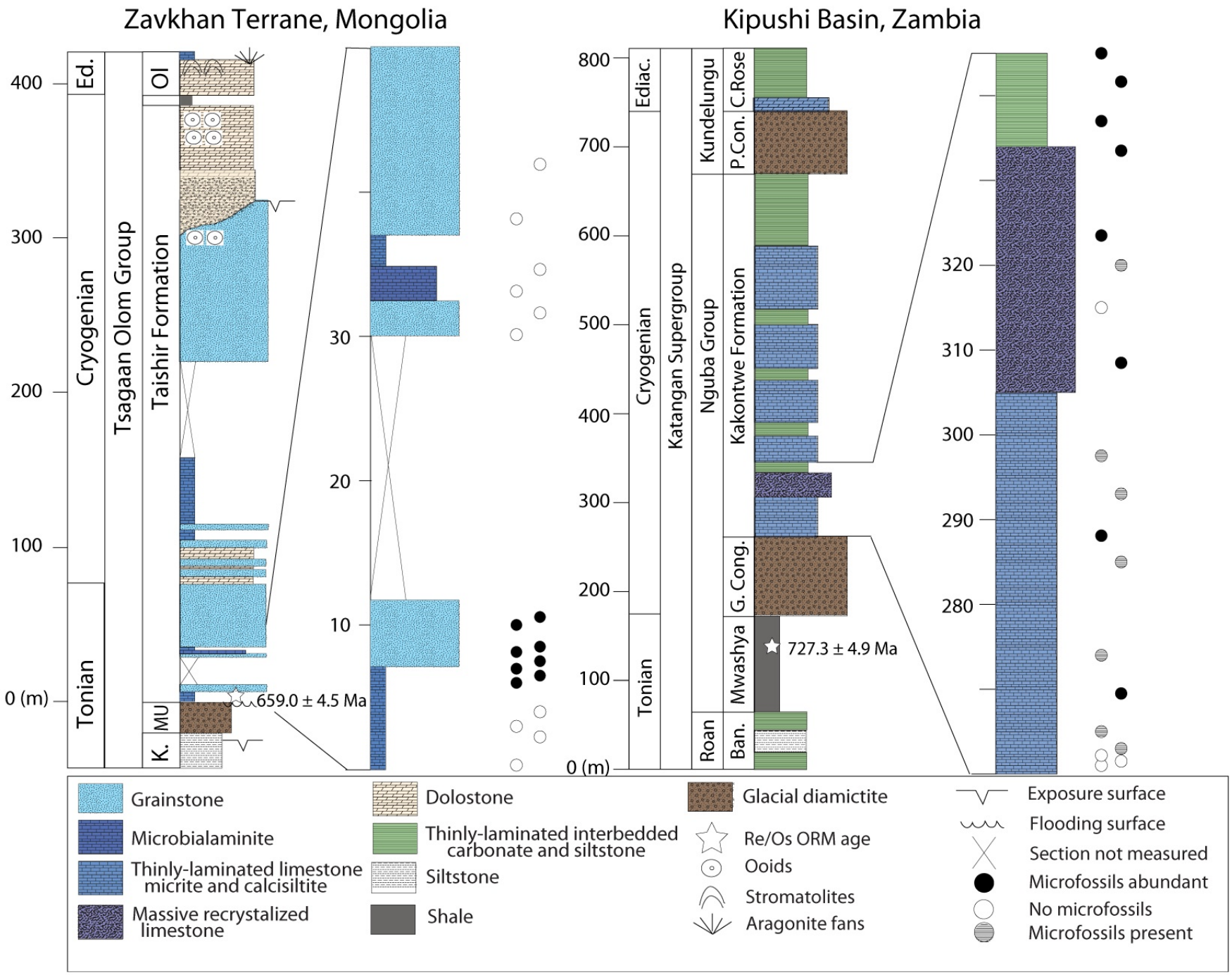
Zavkhan Terrane, Mongolia
Kipushi Basin, Zambia
400
300
200
100
0 (m)
Ed.
Ol
Cryogenian
Tsagaan Olom Group
Taishir Formation
Tonian
MU
K.
659.0 ± 4.5 Ma
30
20
10
800
700
600
500
400
300
200
100
0 (m)
Ediac.
Cryogenian
Tonian
Katangan Supergroup
Kundelungu
P.Con.
C.Rose
Nguba Group
Kakontwe Formation
G. Cong.
Mwashya
Roan
Ban.
727.3 ± 4.9 Ma
320
310
300
290
280
Grainstone
Microbialaminite
Thinly-laminated limestone micrite and calcisiltite
Massive recrystalized limestone
Dolostone
Thinly-laminated interbedded carbonate and siltstone
Siltstone
Shale
Glacial diamictite
Re/Os ORM age
Ooids
Stromatolites
Aragonite fans
Exposure surface
Flooding surface
Section not measured
Microfossils abundant
No microfossils
Microfossils present

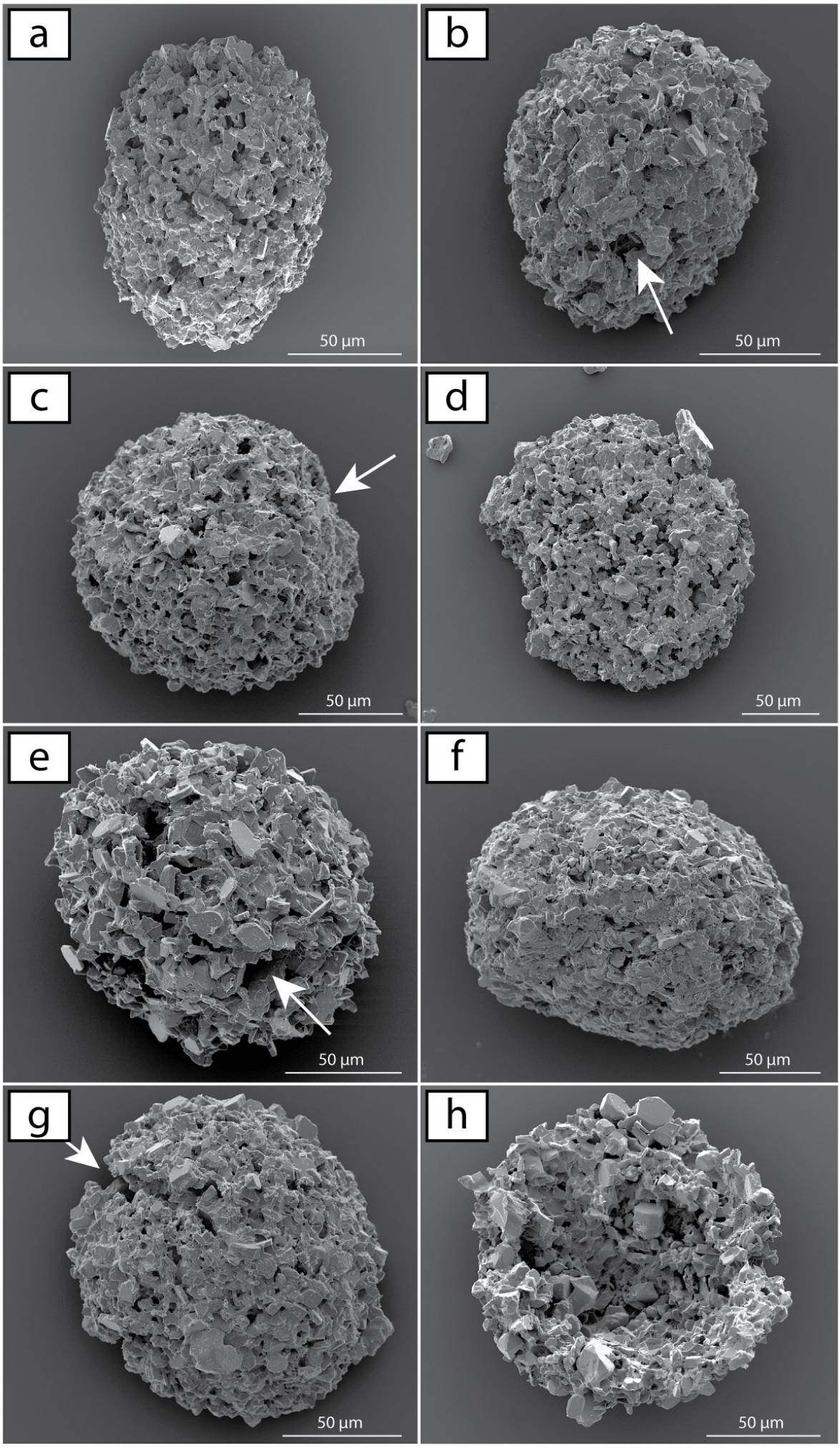
a
50 µm
b
50 µm
c
50 µm
d
50 µm
e
50 µm
f
50 µm
g
50 µm
h
50 µm

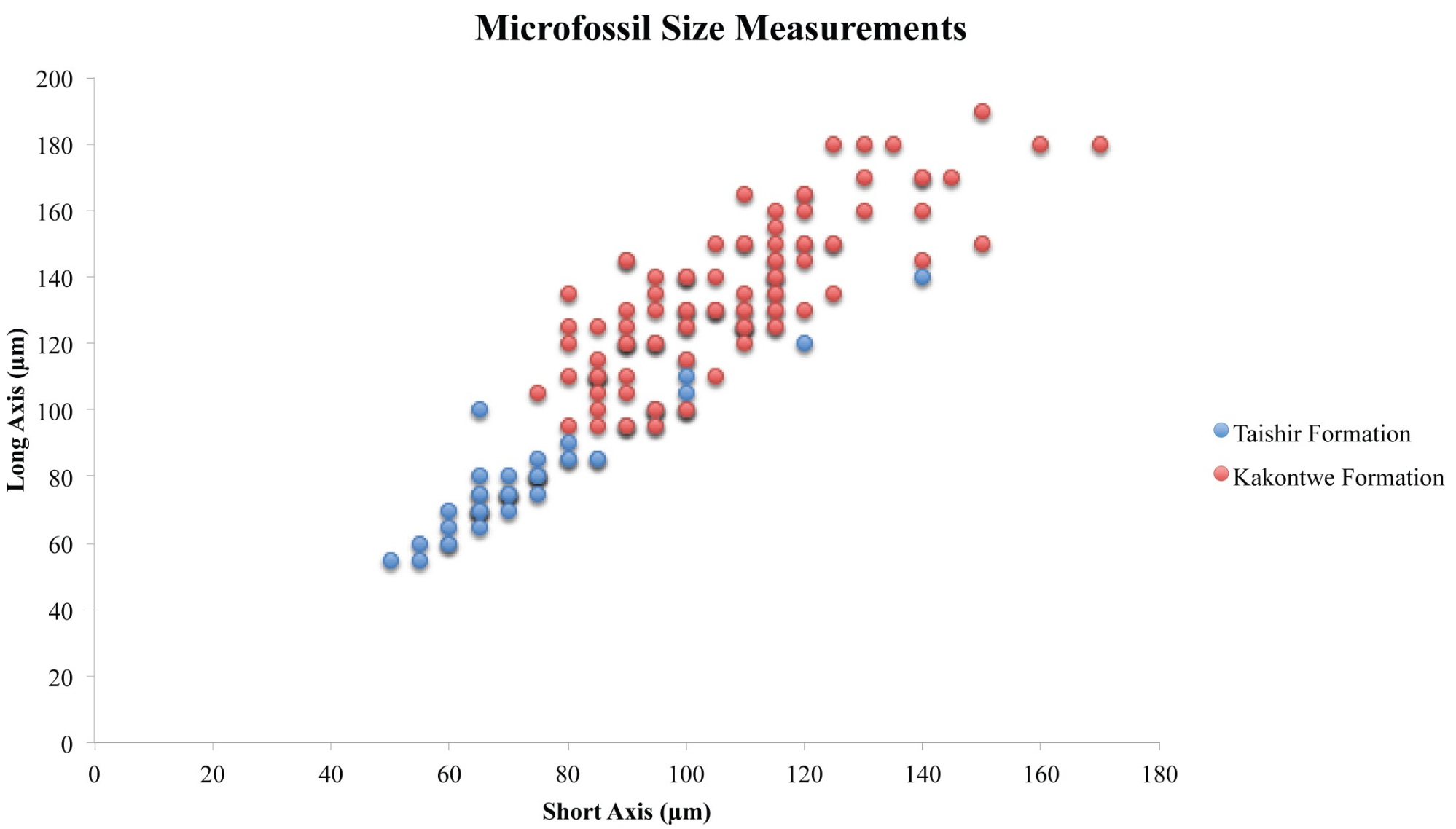
Microfossil Size Measurements
Long Axis (µm)
Short Axis (µm)
0
20
40
60
80
100
120
140
160
180
200
Taishir Formation
Kakontwe Formation

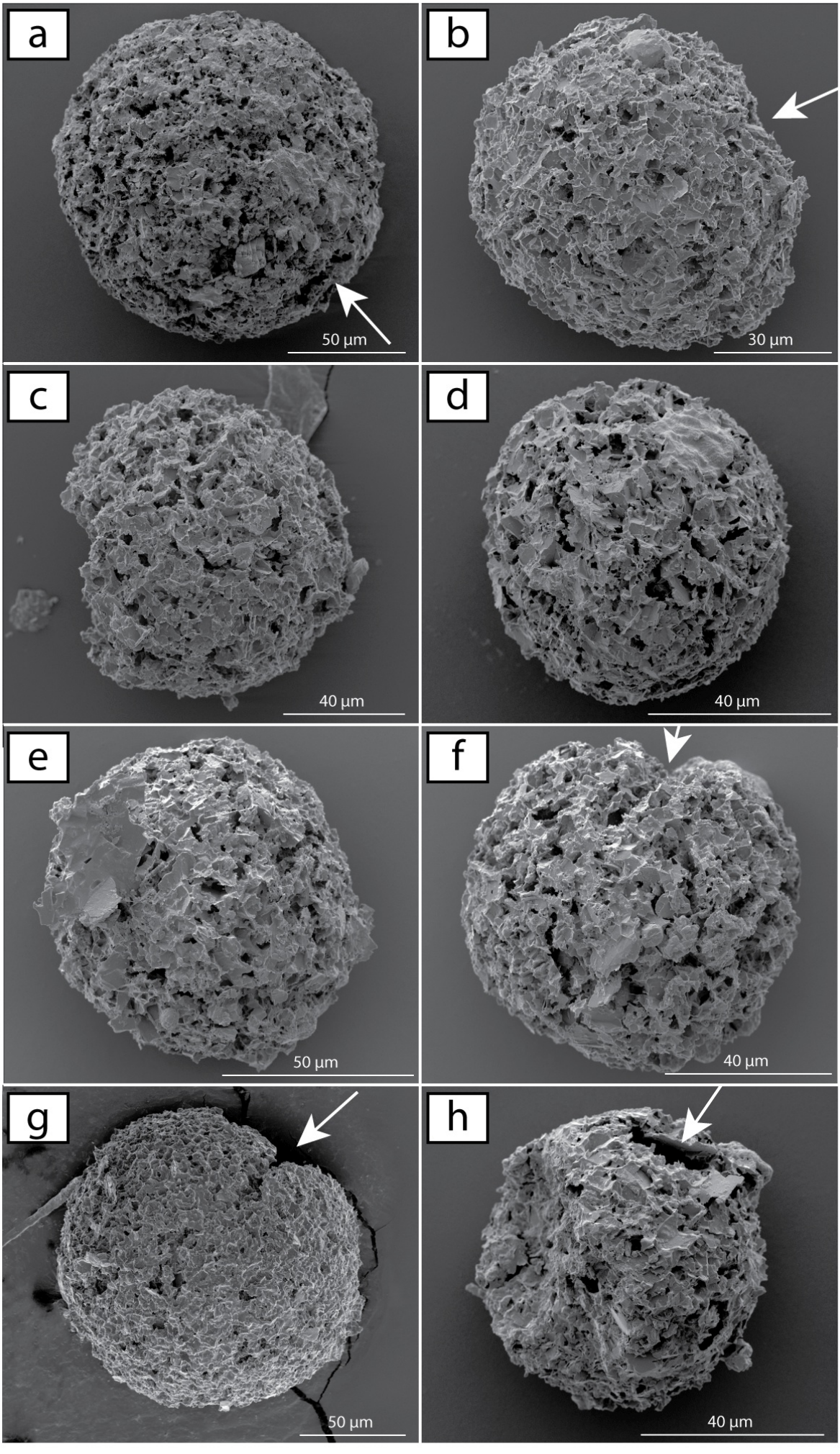
a
50 µm
b
30 µm
c
40 µm
d
40 µm
e
50 µm
f
40 µm
g
50 µm
h
40 µm

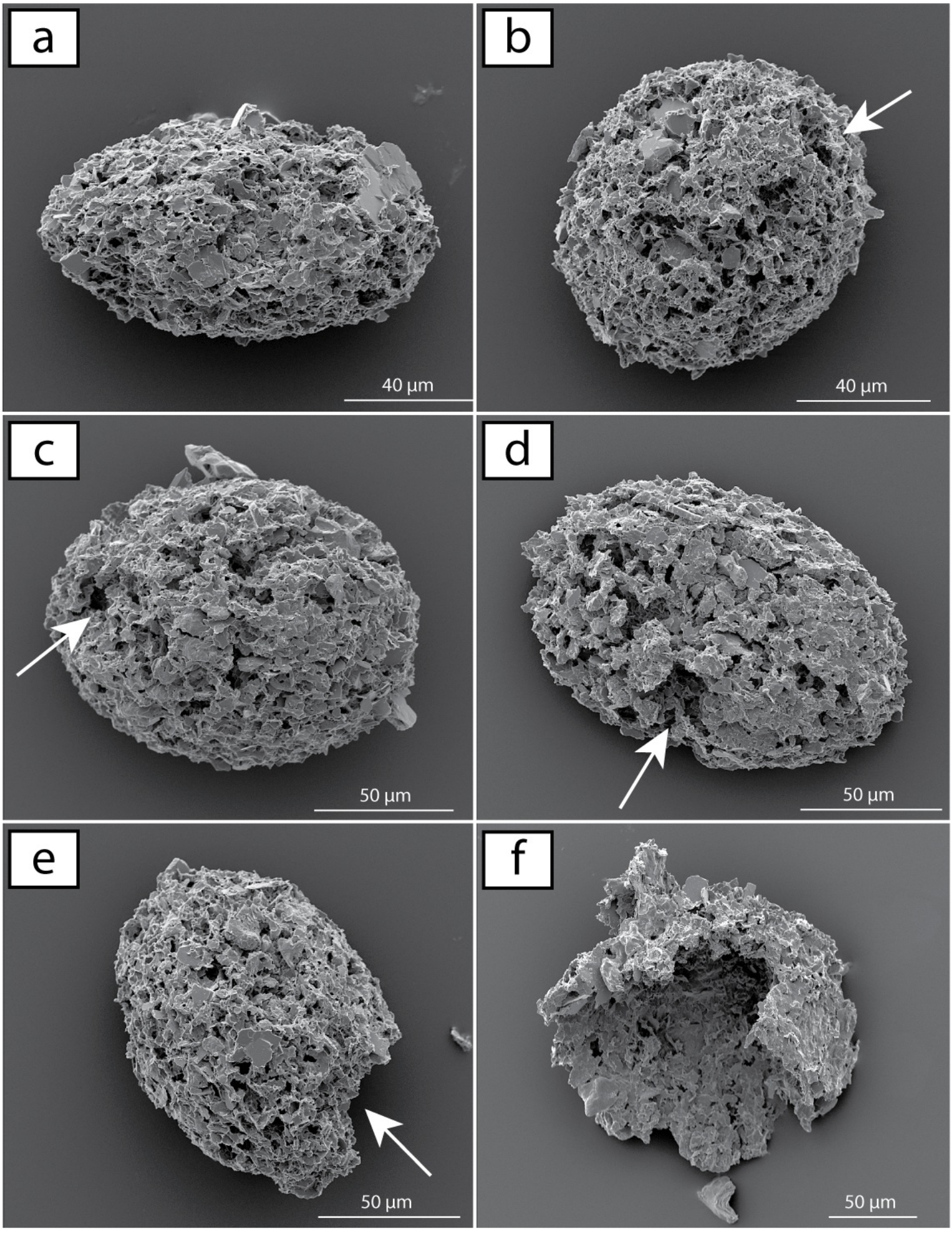
a
40 µm
b
40 µm
c
50 µm
d
50 µm
e
50 µm
f
50 µm

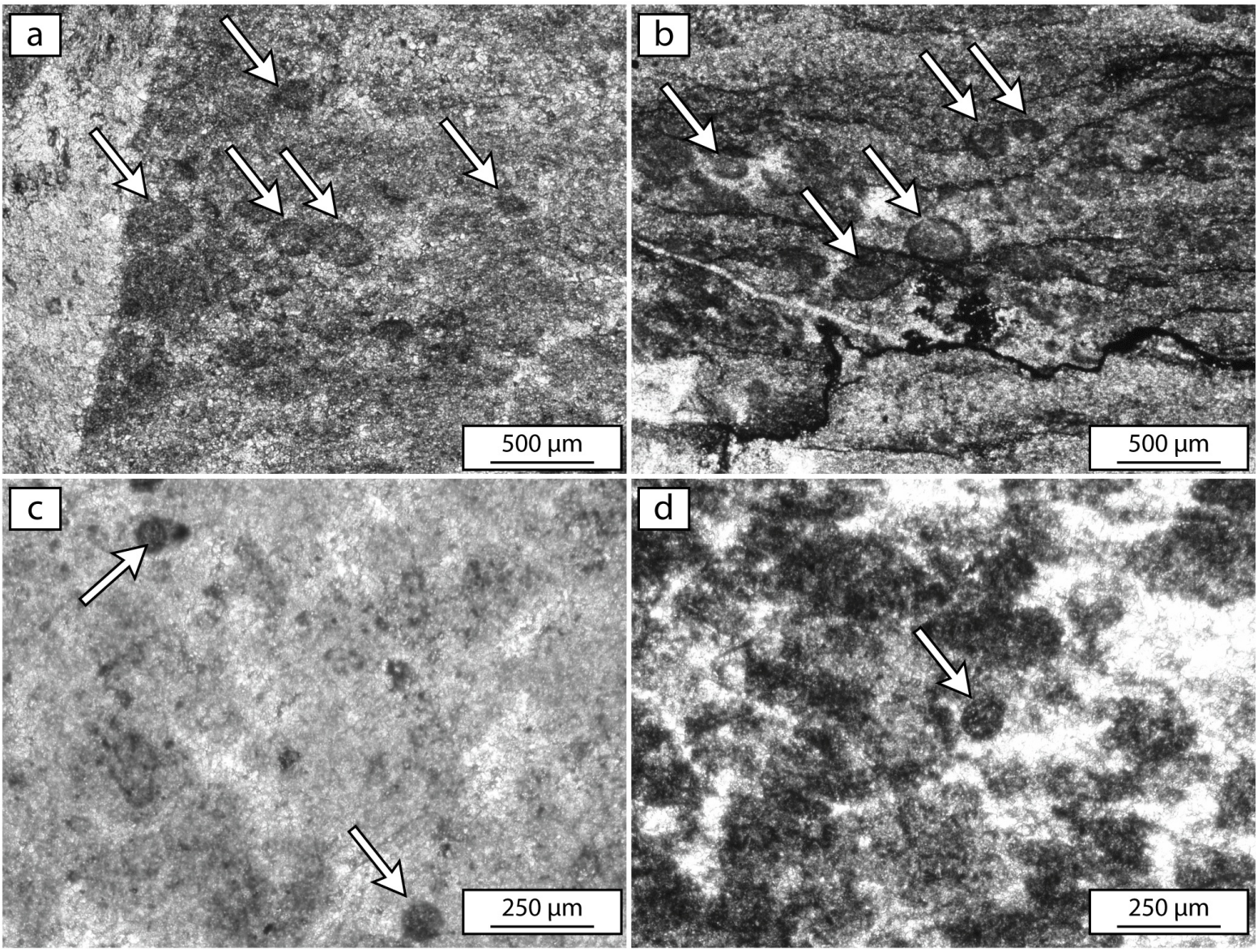
a
500 µm
b
500 µm
c
250 µm
d
250 µm

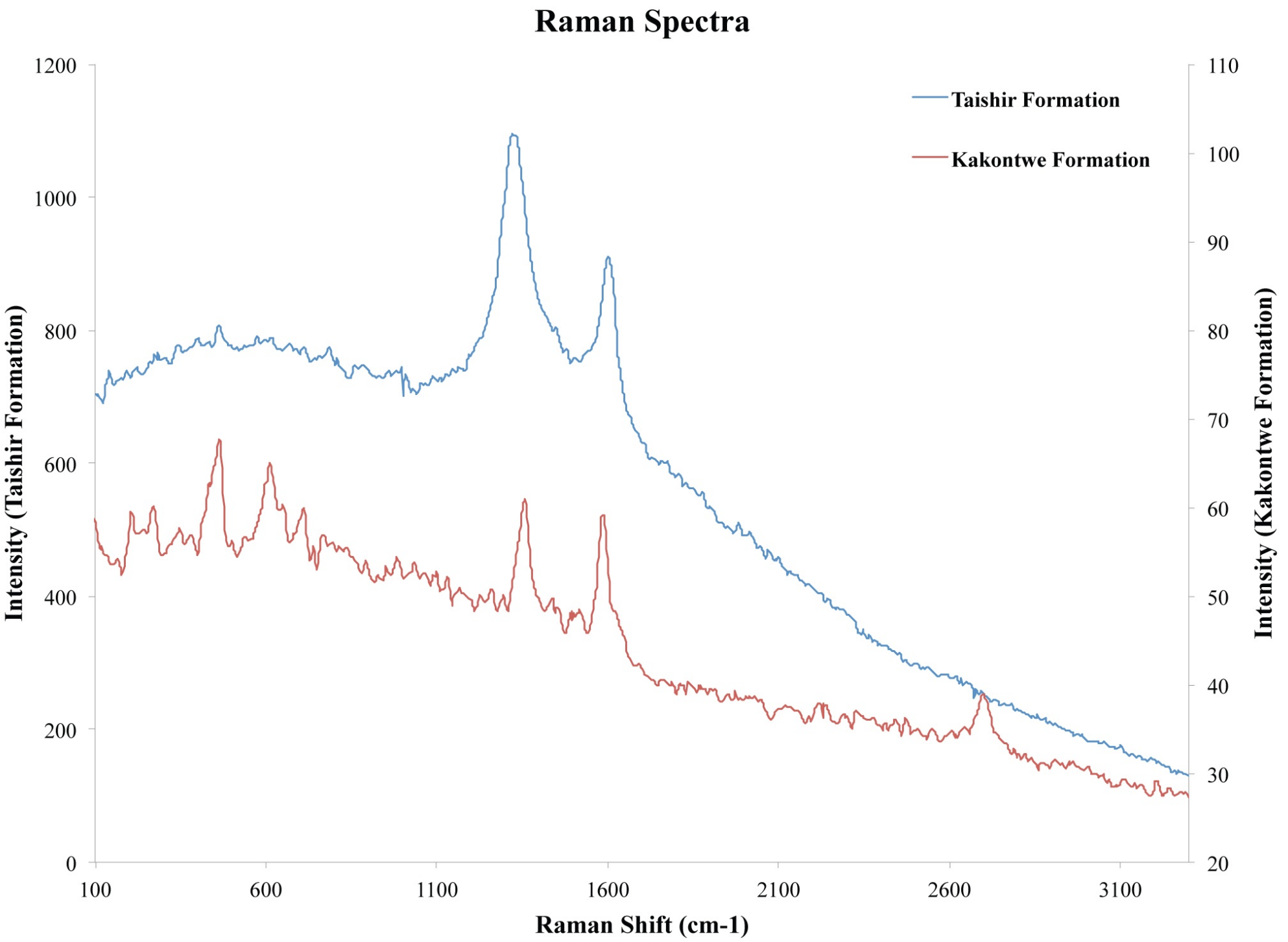
Raman Spectra
Taishir Formation
Kakontwe Formation
Intensity (Taishir Formation)
Intensity (Kakontwe Formation)
Raman Shift (cm-1)
1200
1000
800
600
400
200
0
110
100
90
80
70
60
50
40
30
20
100
600
1100
1600
2100
2600
3100

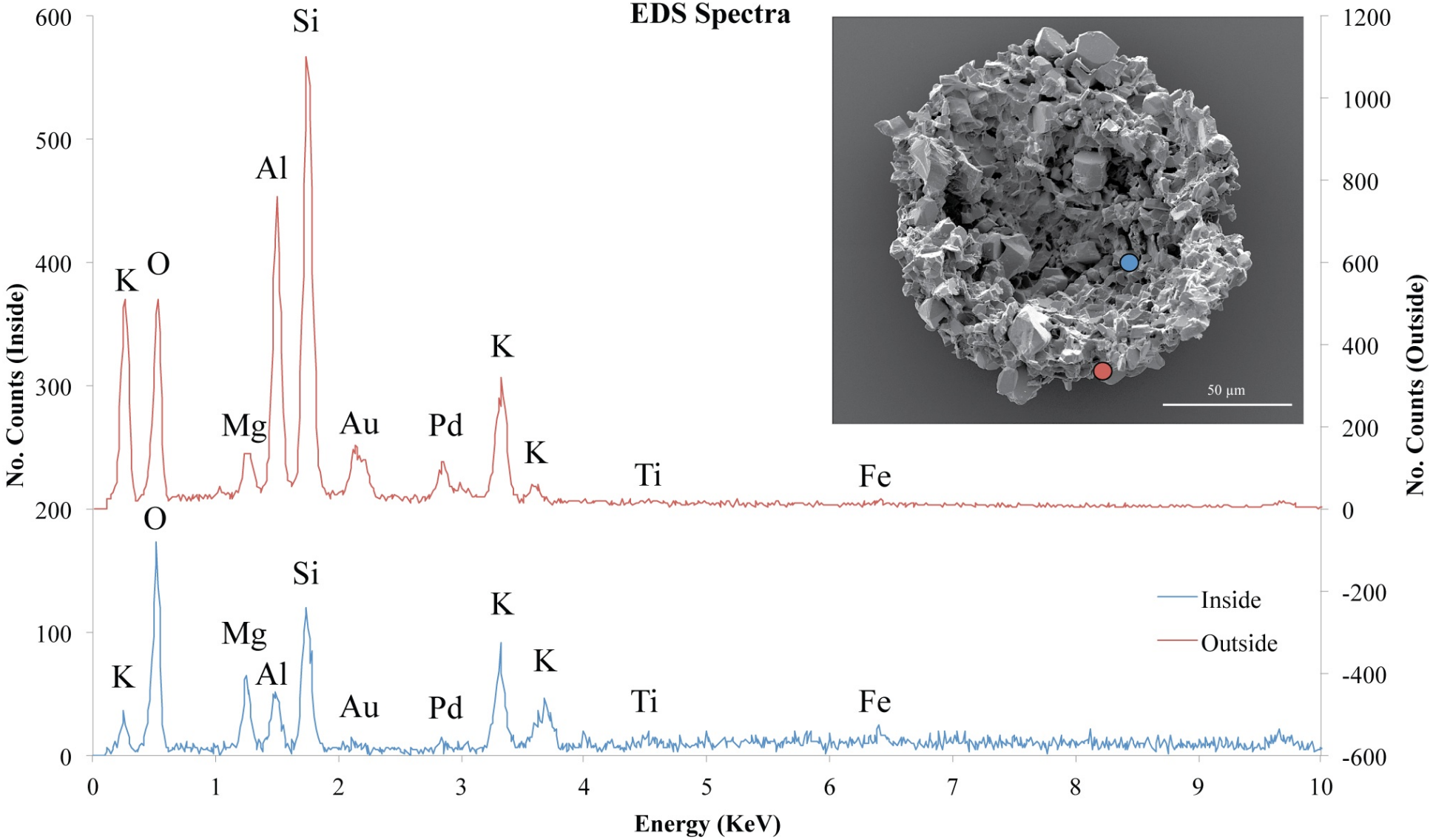
EDS Spectra
No. Counts (Inside)
No. Counts (Outside)
Energy (KeV)
Inside
Outside
50 µm
Si
Al
K
O
Mg
Au
Pd
K
K
Ti
Fe
O
Si
K
Mg
Al
K
K
Au
Pd
Ti
Fe

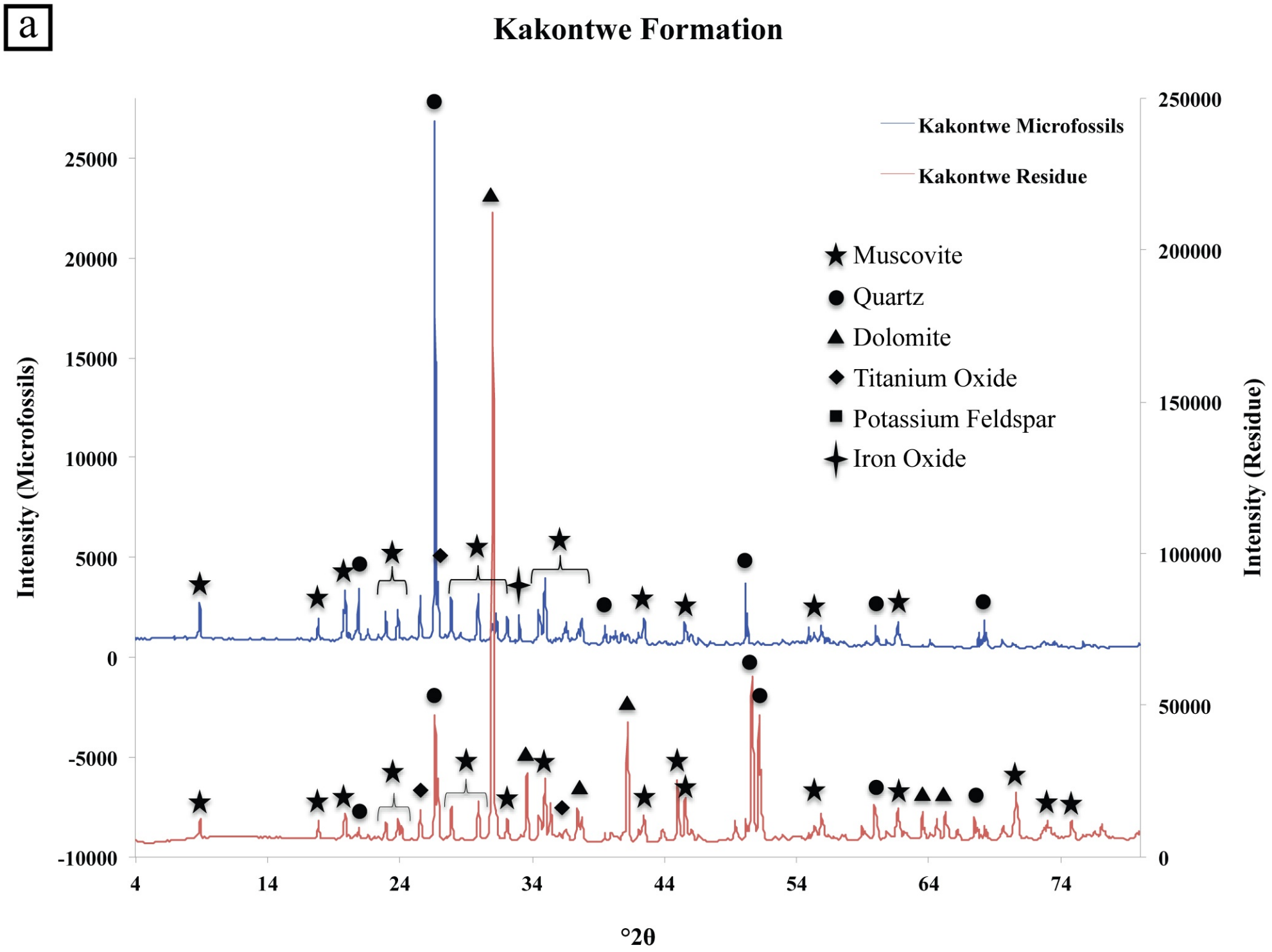
a
Kakontwe Formation
Kakontwe Microfossils
Kakontwe Residue
Muscovite
Quartz
Dolomite
Titanium Oxide
Potassium Feldspar
Iron Oxide
Intensity (Microfossils)
Intensity (Residue)
25000
20000
15000
10000
5000
0
-5000
-10000
250000
200000
150000
100000
50000
0
4
14
24
34
44
54
64
74
°2θ

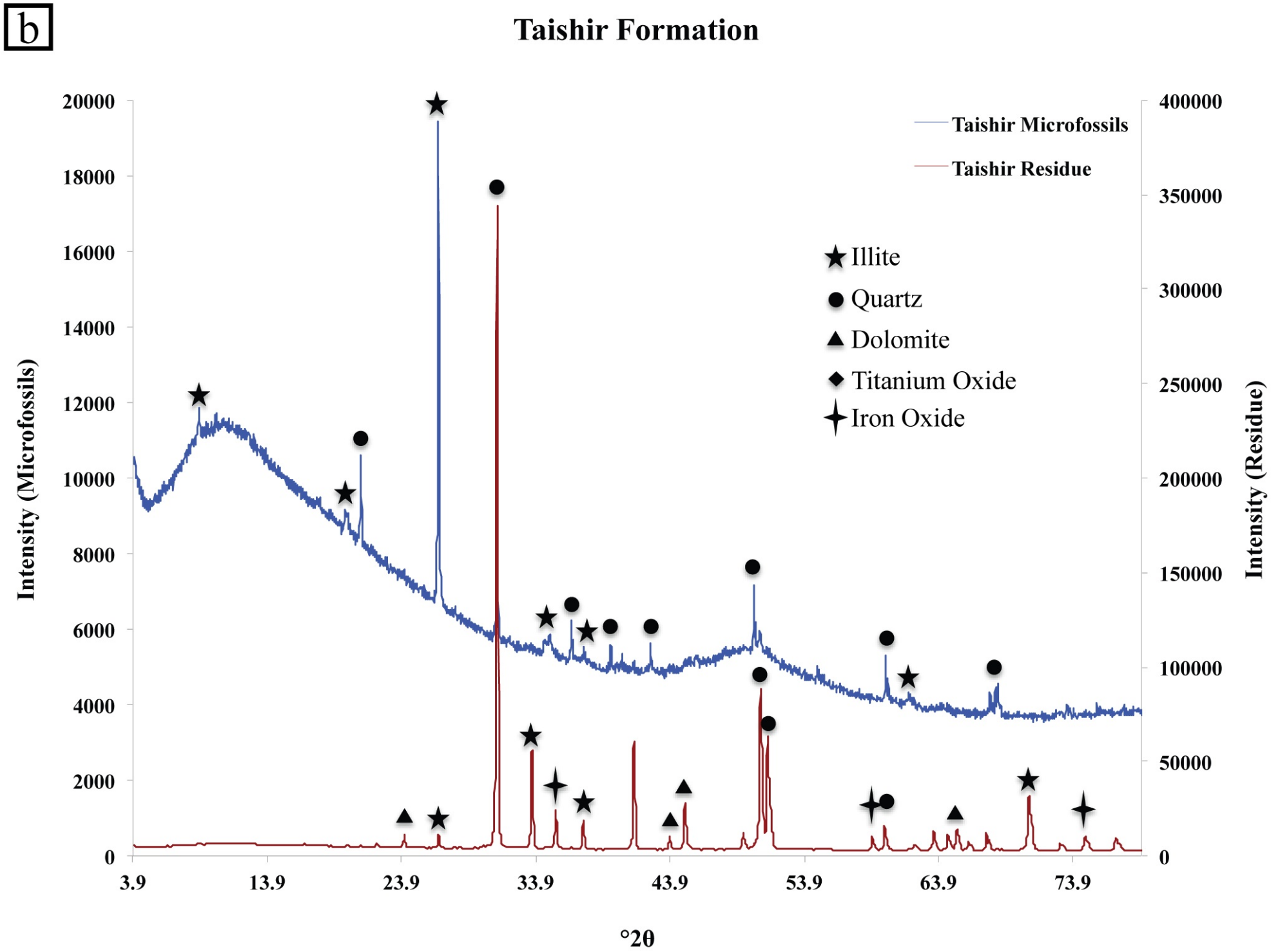
b
Taishir Formation
Taishir Microfossils
Taishir Residue
Illite
Quartz
Dolomite
Titanium Oxide
Iron Oxide
Intensity (Microfossils)
Intensity (Residue)
°2θ
20000
18000
16000
14000
12000
10000
8000
6000
4000
2000
0
400000
350000
300000
250000
200000
150000
100000
50000
0
3.9
13.9
23.9
33.9
43.9
53.9
63.9
73.9

C

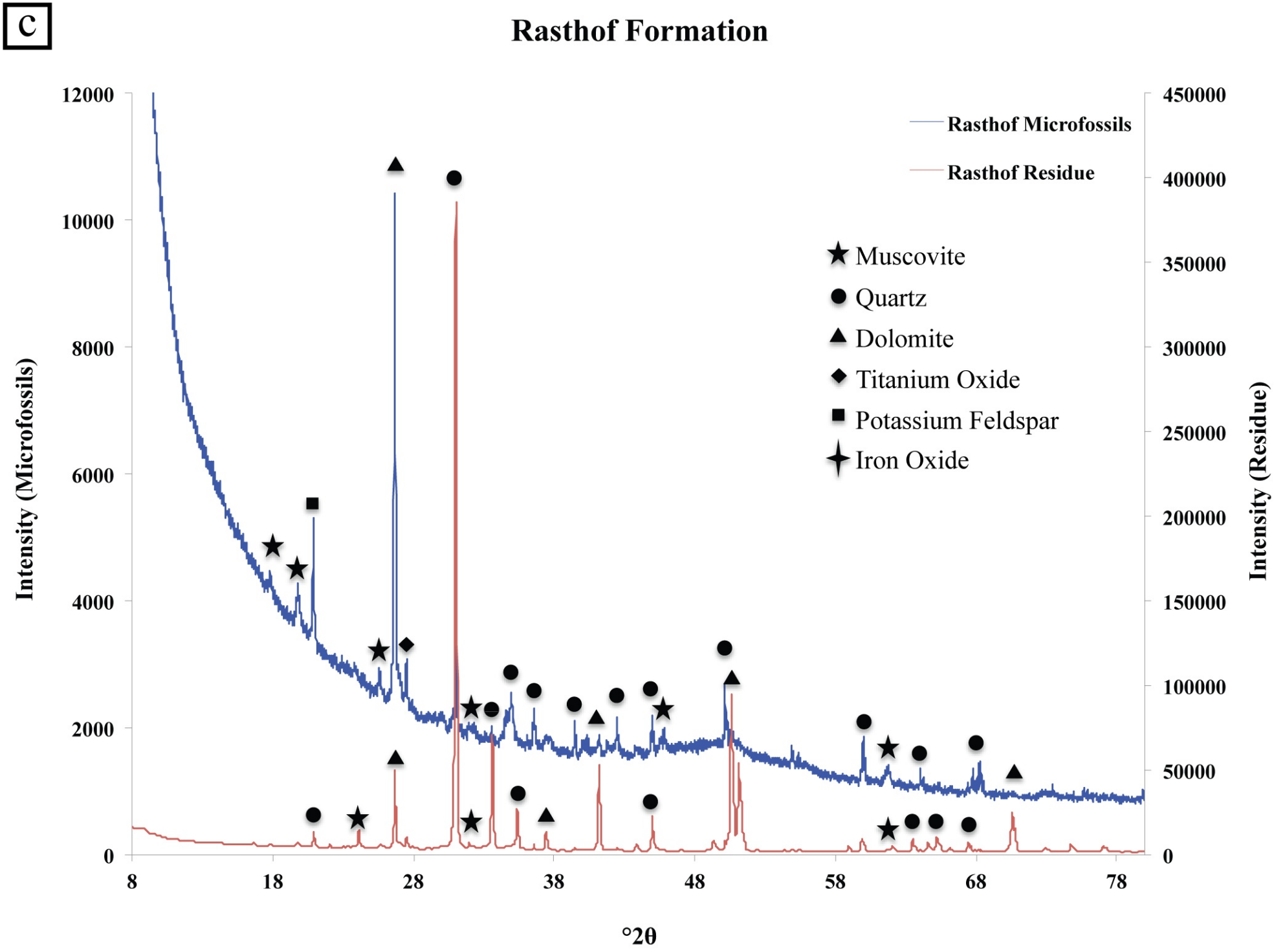
Rasthof Formation
Rasthof Microfossils
Rasthof Residue
Muscovite
Quartz
Dolomite
Titanium Oxide
Potassium Feldspar
Iron Oxide
Intensity (Microfossils)
Intensity (Residue)
°2θ
12000
10000
8000
6000
4000
2000
0
450000
400000
350000
300000
250000
200000
150000
100000
50000
0
8
18
28
38
48
58
68
78

a

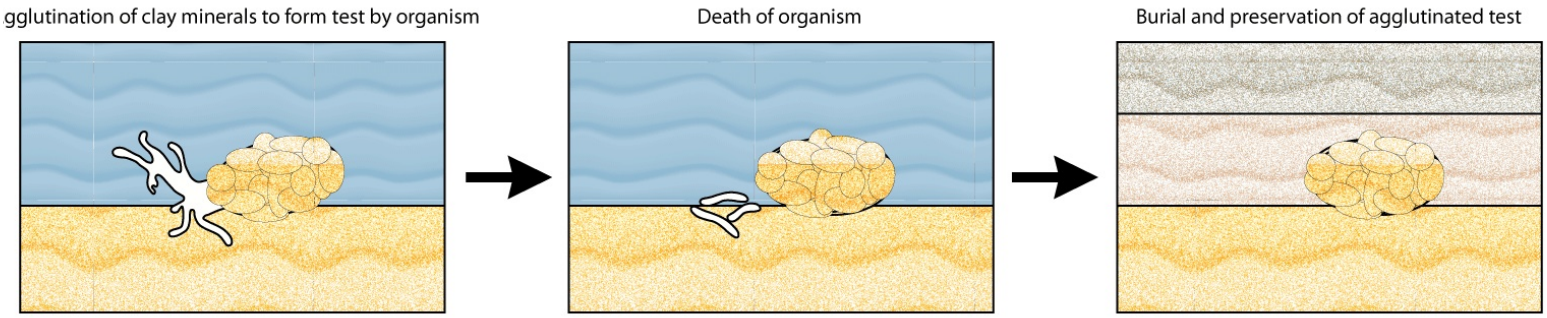
gglutination of clay minerals to form test by organism
Death of organism
Burial and preservation of agglutinated test

b

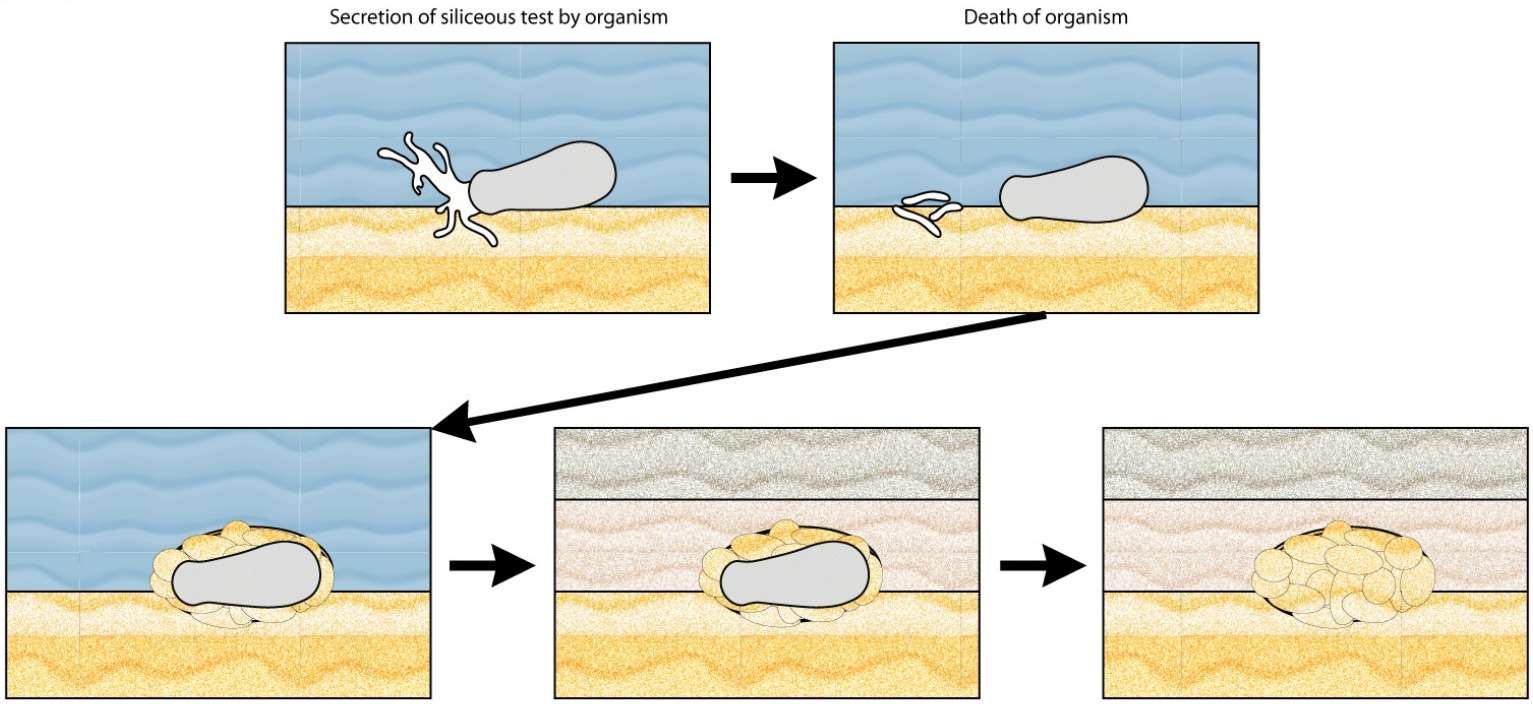
Secretion of siliceous test by organism
Death of organism
dsorption or precipitation of clay minerals around sili-
ceous test
Burial of test and coating of clay minerals
Degradation of siliceous test and preservation of cla
mineral coating

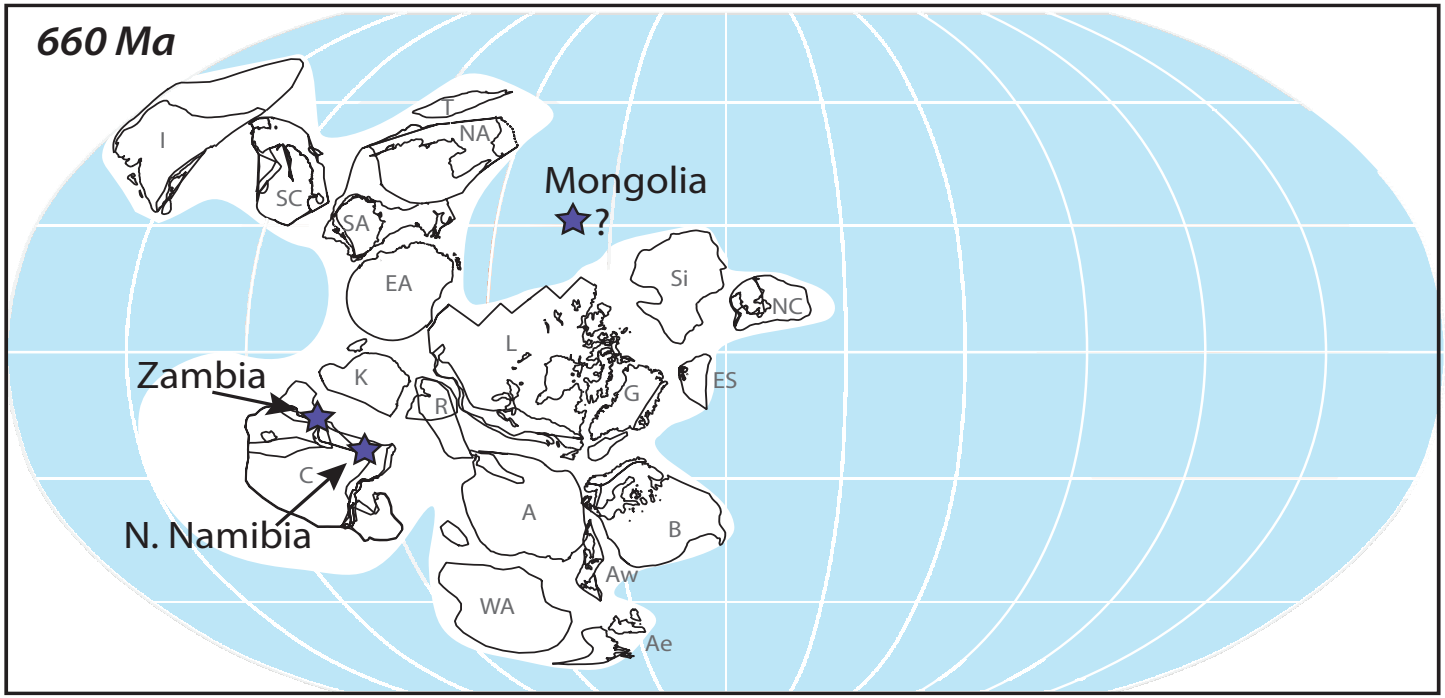
660 Ma
I
T
NA
SC
SA
EA
Mongolia
?
Si
NC
L
K
R
G
ES
Zambia
C
A
B
Aw
WA
Ae
N. Namibia

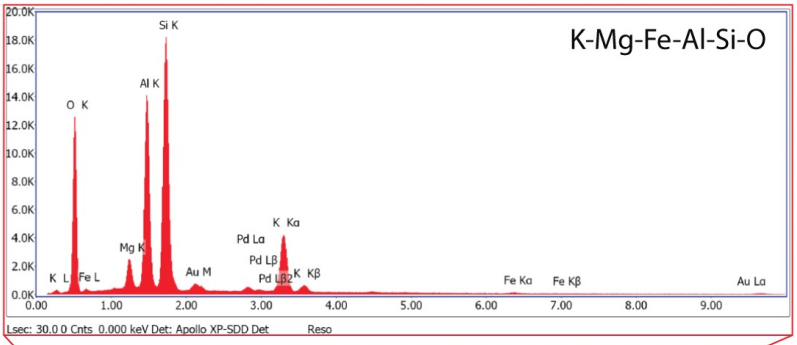
K-Mg-Fe-Al-Si-O
Si K
Al K
O K
Mg K
Au M
K Kα
Pd La
Pd Lβ
Pd Lβ2
K Kβ
Fe Kα
Fe Kβ
Au La
Lsec: 30.0 0 Cnts 0.000 keV Det: Apollo XP-SDD Det Reso

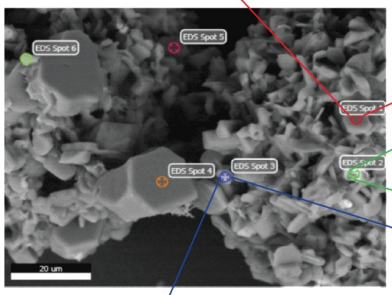
EDS Spot 6
EDS Spot 5
EDS Spot 4
EDS Spot 3
EDS Spot 2
20 um

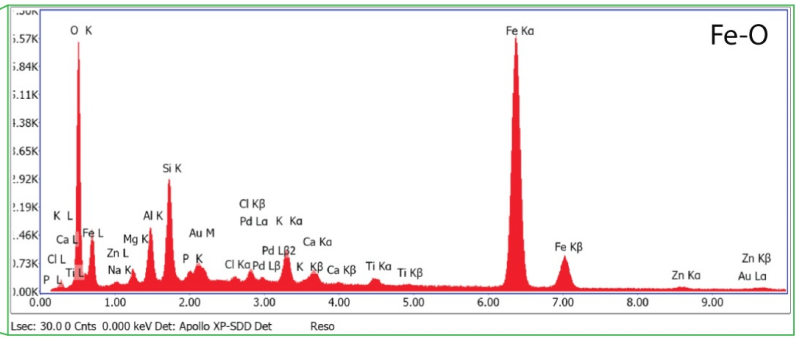
Fe-O
O K
Fe Kα
Si K
Al K
Fe Kβ
Lsec: 30.0 0 Cnts 0.000 keV Det: Apollo XP-SDD Det Reso

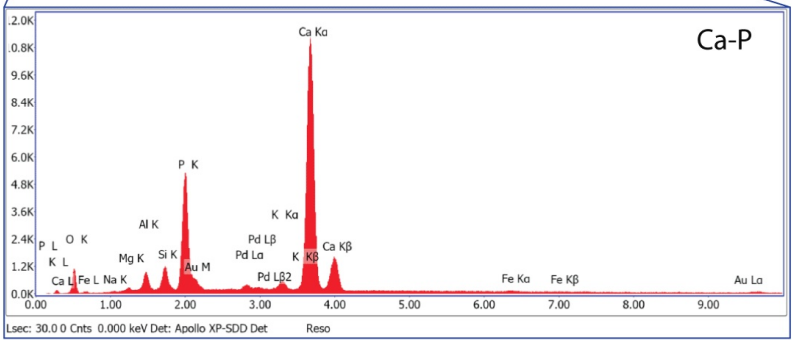
Ca-P
Ca Kα
P K
Al K
K Kα
Ca Kβ
Fe Kα
Fe Kβ
Au La
Lsec: 30.0 0 Cnts 0.000 keV Det: Apollo XP-SDD Det Reso